



Evaluating methods to assess the coastal flood hazard on a global scale

A comparative analysis between the Bathtub approach and the LISFLOOD-AC model

J.Bootsma

**UNIVERSITY
OF TWENTE.**



Evaluating methods to assess the coastal flood hazard on a global scale

A comparative analysis between the Bathtub approach and the LISFLOOD-AC model

Master Thesis

J. Bootsma

University of Twente
IHE Delft Institute for Water Education
April 2022

Cover picture: 3D Sphere and waves of lines geometric abstract by Hi Res

Colophon

This document is a Master Thesis to obtain the degree of Master of Science in Civil Engineering and Management from the University of Twente.

Title	Evaluating methods to assess the coastal flood hazard on a global scale - A comparative analysis between the Bathtub approach and the LISFLOOD-AC model
Author	J. Bootsma
Student number	S1823817
Email	jesse.bootsma@hotmail.com
Version	Final report
Date	27 April 2022
Educational institute	University of Twente Faculty of Engineering and Technology Department of Water Engineering and Management
External organisation	IHE Delft Institute for Water Education Department of Coastal and Urban Risk and Resilience
Supervising committee	
Head of committee	Prof. Dr. R.W.M.R.J.B. Ranasinghe <i>University of Twente</i>
Internal daily supervisor	Dr. Ir. T.M. Duong <i>University of Twente</i>
External daily supervisor	Ir. J. Reyns <i>IHE Delft Institute for Water Education</i>
External committee member	Dr. MEng. MSc. M. Vousdoukas <i>European Commission, Joint Research Centre</i>
Location	Delft, the Netherlands

Preface

This thesis represents the final piece to obtain the MSc title in Water Engineering and Management at the University of Twente. The research project was carried out at IHE Delft Institute for Water Education. Unfortunately, due to the coronavirus, the main part of the project was carried out from home.

First of all, I want to thank my entire graduation committee. I would especially like to thank my daily supervisor, Johan Reyns. The patience of Johan and his advice for any type of issue is something I really appreciated. Furthermore, the regularly planned meetings together with Roshanka Ranasinghe and Trang Duong were of great value to me, both content related as just for a nice chat. Last but not least I would like to thank Michalis Vousdoukas, who guided me through the model set-up and who was always ready to answer any context related questions.

Since I have performed most of this project from my student room in Delft, the support by my roommates really helped me during this period. The coffee breaks on our sun-drenched roof terrace deserve a special notice.

Lastly, I would like to thank my family and friends, from whom I have always received support when needed. The fun and distracting times from the couch, the ice rink or the bike were of great value to me.

I hope you will enjoy reading this thesis report.

Jesse Bootsma

Delft, April 2022

Summary

The already present global coastal flood risk is a threat to population, infrastructure and coastal ecosystems (Vafeidis et al., 2008). Due to changes in storm patterns and sea level rise, a significant increase in coastal flood hazard is expected (Church & Gregory, 2019; Forzieri et al., 2016). Since hazard estimation is a necessary precursor to risk assessment, coastal flood hazard assessment at large spatial scales is needed.

This study investigates global inundation estimations from the Bathtub approach, and critically compares the approach and results to the outcomes of the more detailed, process-based, reduced complexity model LISFLOOD-AC. The LISFLOOD-AC model used for coastal flood inundation estimates on a global scale is a relatively computationally expensive model. The commonly used Bathtub approach does not have this limitation, although this model can overestimate the flood magnitude (Vousdoukas et al., 2016). This study investigates whether the computational time of models can be reduced without compromising on quality of results. The spatial domain of this study involves the entire stretch of coastline around the World. Both models were compared for the baseline period 1980-2014. The model scenarios included span return periods of extreme sea levels from 5 to 200 years. Identifying differences in estimated flood extent was the main task in this project. The flooded area estimates of both modelling approaches were subdivided based on administrative boundaries, coastal typologies and terrain classes. The outcomes were compared as flooded area in (km^2), flooded area normalized by shoreline length in (km^2/km) and as factor difference (Bathtub / LISFLOOD-AC). Trapezoidal numerical integration was applied to the flooded area estimates spanning all baseline return periods to compare the model outcomes as Expected Annual Flooded Areas (EAFA) in ($\text{km}^2/\text{km}/\text{yr}$). Furthermore, the fit metrics: hit rate, false alarm rate, and critical success index were determined for all baseline return periods. In this, the hit rate represents the flooded area correctly predicted by the Bathtub approach, the false alarm rate is a metric of overestimation and the critical success index is a metric of agreement between both modelling approaches.

Results from this study show that the Bathtub modelling approach overestimates the flooded area significantly compared to the process-based reduced-complexity model LISFLOOD-AC. This holds for most countries on Earth (subquestion 1), every coastal typology (subquestion 2) and every terrain class (subquestion 3). The Bathtub approach estimates a global EAFA that is 5.9 times larger than the estimate by the LISFLOOD-AC model. Furthermore, this overestimation was observed for all baseline return periods included, although the factor difference reduced when moving to higher return periods of extreme sea levels. Smaller differences were observed for steeper coastlines, for which the influence of the topography is larger. This results in less overestimation by the Bathtub approach. The propagation of the coastal flood is only limited by the topography in the Bathtub approach, while the LISFLOOD-AC model also incorporates the effect of landscape roughness. Therefore, in flat terrains like plains, the flood propagation in the Bathtub approach experiences no deceleration which causes significant extents of the flood. This especially holds in combination with the fact that the Bathtub approach does not include conservation of mass and therefore assumes an unlimited amount of water that can propagate inland. The hit rates reveal that the Bathtub approach generally estimates flooding in areas where the LISFLOOD-AC model does as well. However, from the false alarm rates it is clearly observed that the Bathtub approach significantly overestimates the flooded area. Lastly, the critical success index values are generally low, representing an insufficient agreement between the flooded area estimates by both modelling approaches. According to the findings of this study, it appears to be ill-advised to use the Bathtub approach in quantitative assessments of the coastal flood hazard at large spatial scales.

Contents

1	Introduction	1
1.1	Theoretical background	1
1.1.1	Coastal flood hazard relation to risk assessment	1
1.1.2	Variables and processes affecting the coastal flood hazard	3
1.1.3	Global coastal hazard modelling	4
1.2	Problem statement	10
1.3	Scope	10
1.4	Objective and research questions	10
1.5	Thesis outline	11
2	Coastal flooding models under study	13
2.1	Bathtub approach	13
2.2	LISFLOOD-AC model	13
2.3	Model set up and input data	15
2.3.1	Spatial domain and coastal segments	15
2.3.2	Model scenarios	15
2.3.3	Extreme sea levels	16
2.3.4	Digital elevation model	17
2.3.5	Flood protection data	17
2.3.6	Synthetic hydrograph	18
2.3.7	Hydraulic roughness values	19
2.4	Comparison of both modelling approaches	19
2.5	Description of model outcomes	19
3	Methodology	21
3.1	Flood data post-processing	21
3.1.1	Matlab to GeoTIFF files	21
3.1.2	Inundation of surface water	22
3.1.3	Reclassifying and area determination	22
3.2	Differences flooded area based on administrative boundaries	23
3.3	Differences flooded area per coastal typology	25
3.3.1	Coastal typology database pre-processing	26
3.4	Differences flooded area per terrain class	27
3.4.1	Terrain classes database pre-processing	28
4	Results	29
4.1	Flood extent based on administrative boundaries	29
4.1.1	Flooded area per country	29
4.1.2	Flooded area per country, normalized by shoreline length	32
4.1.3	Differences in flood extent	33
4.1.4	Global totals	35
4.1.5	Fit metrics	36
4.2	Flood extent per coastal typology	38
4.2.1	Flooded area per coastal typology	38
4.2.2	Fit metrics	40
4.3	Flood extent per terrain class	41
4.3.1	Flooded area per terrain class	41

4.3.2	Fit metrics	43
5	Discussion	45
5.1	Findings and reasoning	45
5.1.1	Country level	45
5.1.2	Coastal typology	45
5.1.3	Terrain classes	46
5.2	Meaning of results	46
5.3	Relation of findings to previously performed research	47
5.4	Limitations of findings	47
5.5	Suggestions for further research	48
6	Conclusion	49
A	Appendices	57
A.1	Derivation and explanation of coastal typologies	57
A.2	Derivation and explanation of terrain classes	61

List of abbreviations

Abbreviation	Definition
CFR	Coastal Flood Risk
GRS	Geographic Coordinate System
DDF	Depth-Damage Function
DEM	Digital Elevation Model
EAD	Expected Annual Damage
EPSG	European Petroleum Survey Group (Geodetic Parameter Dataset)
EAFA	Estimated Annual Flooded Area
ESL	Extreme Sea Level
EVA	Extreme Value Analysis
FA	Flooded Area
GADM	Database of Global Administrative Areas
GCM	Global Climate Model
GSML	Global Mean Sea Level
GHG	Greenhouse Gas
GIA	Glacial Isostatic Adjustment
GIS	Geographic Information System
GSWE	Global Surface Water Explorer
IHE	International Institute for Hydraulic and Environmental Engineering
IPCC	Intergovernmental Panel on Climate Change
JRC	Joint Research Centre
LECZ	Low Elevation Coastal Zone
MSL	Mean Sea Level
NPA	Number of Affected People
RCP	Representative Concentration Pathway
RSLR	Relative Sea Level Rise
SSP	Shared Socioeconomic Pathway
TWL	Total Water Level
UT	University of Twente
WRI	World Resources Institute

1 | Introduction

The already present global coastal flood risk is a threat to population, infrastructure and coastal ecosystems (Vafeidis et al., 2008). The World's climate is changing and extreme meteorological events have a stronger footprint on everyday lives, compared to previous decades (Vousdoukas et al., 2016). Besides, the frequency (Fox-Kemper et al., 2021) and magnitude (Ranasinghe et al., 2021) of coastal floods is expected to increase under all climate change scenarios. Coastal areas around the world are home to a large part of the World's population and the density of valuable assets is typically high. Since a large part of the World's population lives in so-called Low Elevation Coastal Zones (LECZs), the attention for flood risk management is growing. At present, an estimated 1.3% of the global population is prone to a 1-in-100-year flood (Muis et al., 2016) from which 40 million people live in the World's main port cities (Hanson et al., 2011). Socio-economic activity and urban assets cause that LECZs face potentially large consequences due to coastal flooding. With the projected sea level rise and climate-related changes in storm events, the probability of these areas to be flooded and the magnitude of the flooded area becomes bigger (Vousdoukas et al., 2020). Therefore, the attention for coastal flood risk among the scientific community, stakeholders, governments and the public is rising (Vousdoukas et al., 2016). Broad scale assessments of the current and future coastal flood risk are required to cope with this risk, by informing a range of policy decisions (Hinkel et al., 2021). Therefore, a fast, global quickscan of the flood hazard will help to examine the areas for which further locally performed investigation is required. In this way, the need and the extent for possible adaptation strategies can be determined.

1.1 Theoretical background

To provide essential background information about coastal flood hazard assessment and modelling, a literature review is performed. This study ends at the flood hazard level. However, information about flood risk assessment is briefly provided in the literature review since the flood hazard is closely related to the estimated flood risk.

1.1.1 Coastal flood hazard relation to risk assessment

Hazard estimation is a necessary precursor to risk assessment. In general, risk assessment includes the components: hazard, exposure and vulnerability (Reisinger et al., 2020). From the work of numerous researchers, the IPCC (2012) combined their work and came up with the following descriptions of hazard, exposure and vulnerability:

- **hazard** refers to the possible, future occurrence of natural or human-induced physical events that may have adverse effects on vulnerable and exposed elements;
- **Exposure** refers to the inventory of elements in an area in which hazard events may occur;
- **Vulnerability** refers to the propensity of exposed elements such as human beings, their livelihoods, and assets to suffer adverse effects when impacted by hazard events (IPCC, 2012)

The components of disaster risk and its connection with climate and socioeconomic processes is presented in Figure 1.1.

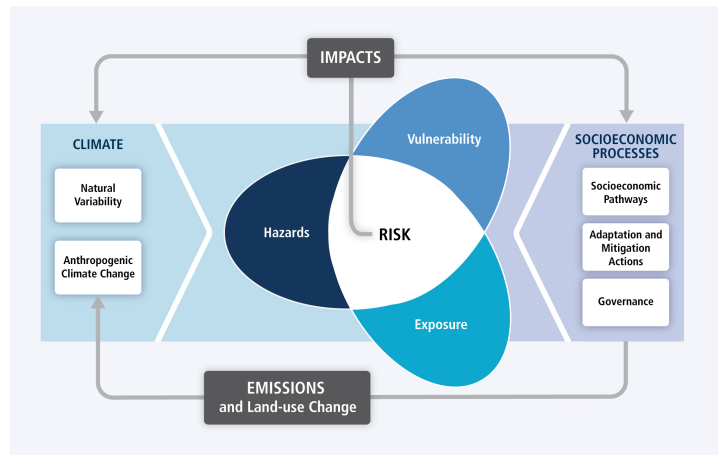


Figure 1.1: Climate-related risk as a result of the interaction of climate-related hazards, with vulnerability and exposure of human and natural systems. Drivers of hazard, exposure and vulnerability include socioeconomic processes and changes in the climate system (IPCC, 2021).

Coastal flood risk assessment

Assessment of the global coastal flood risk is essential under the projected changes in climate, population and socioeconomic activity. Better understanding of the flood risk in flood-prone areas will help inform climate policy and disaster risk (Scussolini et al., 2016).

During recent years, an upscaling has taken place of the scale at which coastal flood risk assessments are performed i.e. from regional and national scale to larger, (inter)continental and global scale. These broad scale assessments are useful in hotspot identification, support for international policymaking and harmonization of climate change adaptation strategies (Vousdoukas et al., 2018a).

Broad scale coastal flood risk assessments inform a range of policy decisions including (Hinkel et al., 2021):

1. Setting global mitigation targets in the context of the United Nations Framework Convention on Climate Change (UNFCCC) to avoid dangerous interference with the climate system (UNFCCC, 1992);
2. Informing Global Assessment Reports on Disaster Risk Reduction by the United Nations Office for Disaster Risk Reduction (UNDRR, 2019);
3. Designing global financial mechanisms for adaptation (United Nations Environment Programme (UNEP), 2016), disaster relief and loss & damage (Jongman et al., 2014);
4. Strategic long-term development and adaptation planning (Hinkel et al., 2021).

More or less similar to the disaster risk management components, coastal flood risk (CFR) can be divided in four components which follow the risk definition of the IPCC (Chen et al., 2021; Oppenheimer & Glavovic, 2019). The four components of CFR are as follows:

1. **Mean and extreme sea-level hazards**, including sea-level rise, tides, surges, waves, river run-off and their interactions;
2. **Hazard propagation** onto the shore and the floodplain, including interaction with natural (e.g. dunes) and artificial (e.g. dikes) defences;
3. **Exposure** in terms of area, people and coastal assets potentially threatened by these hazards;
4. **Vulnerability**, which refers to the propensity of the exposure to be adversely affected by the flood hazard (IPCC, 2014a).

All these four components require intensive research and collaboration of multiple experts. The currently used approaches to assess the global coastal flood risk is described in the following chapter. Since this study ends at the third CFR component at the area level, no attention is devoted to the last component involving vulnerability. Furthermore, as only baseline return periods are included in this study, no attention is paid to climate and socioeconomic changes.

1.1.2 Variables and processes affecting the coastal flood hazard

The coastal flood hazard is affected by several processes. The most important ones are presented in this section.

Low Elevation Coastal Zones

The Low Elevation Coastal Zone (LECZ) is described as "*the area below 10m that is hydrologically connected to the ocean*" (Hinkel et al., 2021). This region is home to around 10 % of the world's population and 13 % of the total urban area (Kirezci et al., 2020; McGranahan et al., 2007). This area generates approximately USD 1 trillion of global wealth (Kirezci et al., 2020). In the main port cities around the World, already 40 million people and USD 3 trillion worth of assets are exposed to coastal floods (Hanson et al., 2011). Due to urbanization, wealth- and population growth, this trend is expected to continue in the future under the different socio-economic pathways (Vousdoukas et al., 2020). The population of the LECZ is predicted to rise from 625 million in 2000 to between 879 and 949 million in 2030, eventually approaching 1.4 billion in 2060. (Neumann et al., 2015).

Climate change

During recent years observations made clear that our climate system is changing. Compared to the late 19th century: global mean surface temperature increased; the upper ocean (above 700 m) has warmed; the Earth has been in radiative imbalance receiving more energy from the Sun than reflecting through the atmosphere; the Arctic ice extent decreased and world-wide glaciers shrunk (IPCC, 2021). Under these changing conditions, the stresses on our society increase significantly. As Vousdoukas et al. (2016) stated: "*During recent years, our societies have witnessed several extreme meteorological events which have raised public awareness of the fact that the climate is constantly changing and having a stronger footprint on everyday lives compared to previous decades.*" The future episodic coastal flooding is one of the main disaster risks of our future generation since any climate change driven variation in frequency and/or magnitude of storm events has a significant impact (Kirezci et al., 2020). Together with mean global sea level rise this increases the coastal flood hazard that society is facing.

Global mean sea level rise

From tide gauges and altimetry observation, it is clearly seen that the global mean sea level (GMSL) is rising at an accelerating pace. The global mean sea level increased by 0.20 m between 1901 and 2018. As stated in the Sixth Assessment Report by the IPCC (2021): "*The average rate of sea level rise was 1.3 [0.6 to 2.1] mm yr⁻¹ between 1901 and 1971, increasing to 1.9 [0.8 to 2.9] mm yr⁻¹ between 1971 and 2006, and further increasing to 3.7 [3.2 to 4.2] mm yr⁻¹ between 2006 and 2018 (high confidence).*" Furthermore, it is likely that global mean sea level will rise in the range of 0.28 to 1.01 m (very low GHG emissions scenario to very high GHG emissions scenario) by the end of the 21st century, compared to 1995 to 2014 (IPCC, 2021). The global mean sea level rise per scenario is presented in Figure 1.2.

The increasing sea levels are the result of various processes, of which thermal expansion, ice mass-loss from glaciers and icesheets in Greenland and Antarctica are contributing the most (Vousdoukas et al., 2018c). Furthermore, coastal sea levels will be influenced by vertical land motion (VLM), which is induced by a variety of factors, including glacial isostatic adjustment (GIA) (Vousdoukas et al., 2018c).

Sea level rise is often referred to as relative sea level rise (RSLR), since the sea level is both dependent on the water level as the level of the land itself. This land level can change due to processes like subsidence. RSLR includes the effects of atmospheric loading, land ice, glacial isostatic adjustment, vertical land motion and terrestrial water sources (Fox-Kemper et al., 2021). The change in relative sea level can be significantly different from the global mean sea level due to changes in the distribution of water in the ocean, vertical movement of the land and changes in the Earth's gravitational field (Fox-Kemper et al., 2021).

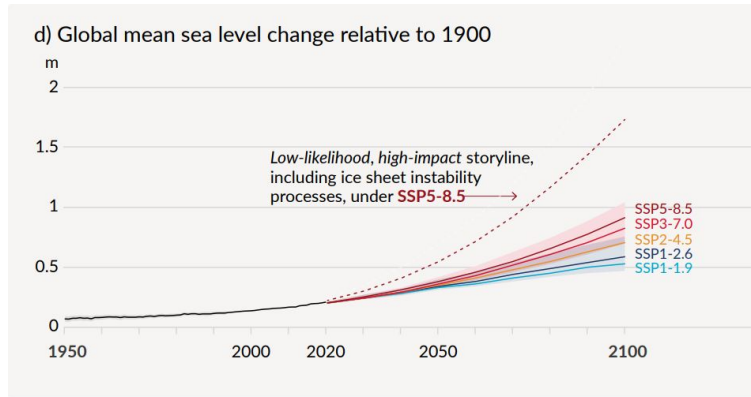


Figure 1.2: Global mean sea level change in metres, relative to 1900. The black curve represents the observations and the projections for the SSP (Shared Socioeconomic Pathways (IPCC, 2021)) scenarios are shown in colour, with the shades representing uncertainty. The projections are based on CMIP (Coupled Model Intercomparison Project), ice-sheet and glacier models. The dashed curve indicates the potential impact of deeply uncertain processes, showing the 83rd percentile of SSP5-8.5 projections including low-likelihood, high-impact ice-sheet processes. Only likely ranges are assessed for SSP1-2.6 and SSP3-7.0. The observed global mean sea level rise from 1900 to 1995-2014 of 0.158 m is added to simulated and observed changes relative to 1995-2014 to calculate changes relative to 1900 (IPCC, 2021).

Extreme sea levels

Related to climate change, the focus is often on mean global sea level rise. However, the major threats of coastal flooding and erosion are significantly impacted by episodic storm surge and wave setup (Kirezci et al., 2020; Paprotny et al., 2019; Vousdoukas et al., 2018c). Their time of occurrence in relation to the astronomical tide is crucial in this.

The definition of an extreme sea level (ESL) is defined by Fox-Kemper et al. (2021) as: *"an exceptionally low or high local sea-surface height arising from combined short-term phenomena (e.g. storm surges, tides and waves)"*. The extreme sea levels relevant for the assessment of the coastal flood hazard are the exceptionally high ones. The contribution of waves to the extreme water level is often not taken into account in large-scale coastal flood hazard assessment since it requires information on the beach-face slope and wave related water level fluctuations take place at smaller temporal scales than the other ESL components. A typical extreme sea level (ESL) equation is as follows:

$$ESL = MSL + \eta_{tide} + \eta_{CE} \quad (1.1)$$

, with MSL the mean sea level, η_{tide} the high tide water level and η_{CE} the water level fluctuations due to climate extremes (waves set up and storm surge by wind)

The frequency of ESLs to occur is expressed as the return period. For example, a commonly used water level in coastal flood hazard assessment is the 1-in-100-year water level (ESL_{100}) which means that this water level has a return period of 100 years. The global average ESL_{100} progressively increases with time and GHG-forcing. Previously performed research by Vousdoukas et al. (2018c) on the extreme sea level projections showed a very likely increase (5-95th percentile) of the global average ESL_{100} with 14-34 cm under RCP4.5 (Relative Concentration Pathways (IPCC, 2014b)) and 24-41 cm under RCP8.5. At the end of the 21st century the increase is expected to be 34-76 cm under RCP4.5 and 58-172 cm under RCP8.5. These values are not spatially homogeneous, but vary considerably on regional scales (Vousdoukas et al., 2018c).

1.1.3 Global coastal hazard modelling

In this chapter, the current modelling practices, the typical model outcomes and the inherent limitations, uncertainties and bias are described. The chapter ends with inundation modelling

techniques and a brief comparison between the static Bathtub approach and the dynamic, process-based, reduced complexity LISFLOOD-AC model, which is part of the LISFLOOD-FP model by Bates and De Roo (2000).

Current practice

To assess the global coastal flood hazard, firstly the extreme water levels should be determined for several return periods. The corresponding flood hazard then transports onto the shore and when protection levels are not sufficient, it propagates landwards. The resulting flood extent with inundation depth will potentially cause severe damage and will be a threat to people in the flood-prone area. A schematic overview of the methodological approach to estimate the coastal flood hazard is presented in Figure 1.3.

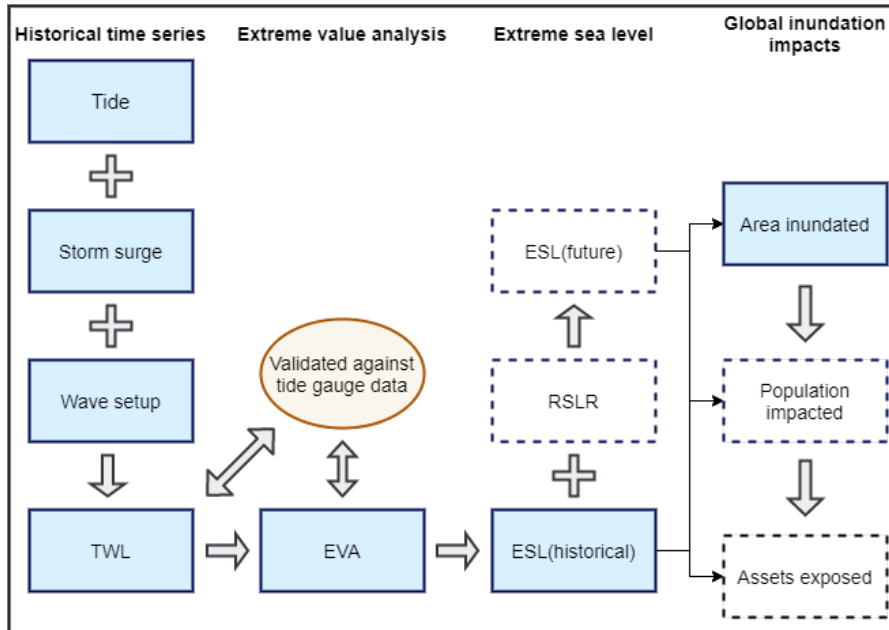


Figure 1.3: Schematic overview of the methodological approach, adapted from (Kirezci et al., 2020). With TWL being the Total Water Level, consisting of tides, storm surge and wave setup. EVA, Extreme Value Analysis, is performed to determine historical extreme sea levels (ESLs) based on the historical TWL time series. To come to future ESLs a component representing Relative Sea Level Rise (RSLR) is included. Since this study focuses on the baseline period and the inundated area, the future scenarios, population and assets exposed are shown in dashed boxes.

The current practice for the first three CFR components, up to inundated area, will be described in detail in the following subsections.

CFR component 1

To assess the global coastal flood hazard, the water level that causes the flood hazard (i.e. the forcing water level) needs to be distinguished. This forcing water level consists of several components, together characterizing the extreme sea level (ESL). As presented in section 1.1.2 the mean sea level (MSL), mean high tide and storm surge all contribute to this ESL. To establish a historical time series of the extreme sea level (ESL(t)), historical high frequency tide gauge records are used. Furthermore, at ungauged locations model simulations based on climate reanalysis (e.g. ERA5) and climate simulations (e.g. CORDEX) can be applied (Hinkel et al., 2021). In the study by Paprotny et al. (2016), the Delft3D model by Deltares is used to calculate surges, which uses the depth-averaged shallow water equations (Deltares, 2014). Together with satellite altimetry data for the MSL and the mean high tide from e.g. TPX08 model (Egbert et al., 1994), the total water level time series is set up. To calculate return periods for extreme water levels, extreme value analysis is performed. To do so, a probability distribution is fitted to the simulated time series, which makes use of the annual maxima or the Peaks over Threshold approach (Paprotny et al., 2019). After establishing the simulated total water level time series, validation is performed by

comparison with global tide gauge data. However, due to climate related processes, future extreme sea levels will be different than these from the past. Therefore, a component characterizing relative sea level rise is included next to expected changes in storm surge and wave patterns.

The steps to come to the extreme sea levels for the considered return periods are as follows:

1. Establishment of total water level time series by determining MSL, surge and tide components from satellite altimetry observations and model simulations respectively.
2. Fitting a probability distribution to water levels from the model simulations for all time periods. Extreme value analysis is performed to obtain statistical estimates of extremes. A probability distribution can be fitted to annual maxima to obtain return periods. Another method is to use all storm peaks above a specified threshold (the Peaks over Threshold approach) (Paprotny et al., 2019).
3. Validation of the simulated TWL time series is performed through comparison with global tide gauge data (Paprotny et al., 2019).
4. To obtain future projections of extreme sea levels, the relative sea level rise is included. This can be integrated with a stationary and a non-stationary approach. The stationary approach (also known as mean sea level offset) just adds a component for RSLR to the historical values (present-day extreme sea level). The magnitude of RSLR differs per RCP of the IPCC and shows regional variability. The non-stationary (or dynamic) approach makes use of hydrodynamic and/or wave models forced with global climate model derived atmospheric fields. Changes in tidal, storm surge and wave distribution are then combined with RSLR projections to obtain future ESLs (Fox-Kemper et al., 2021).

CFR component 2

The flood hazard resulting from the extreme water levels determined under CFR component 1 propagates onto the shore and the floodplains where it interacts with natural (e.g. dunes) and artificial (e.g. dikes) defences.

The current practice is to divide the total coastline of interest in discrete coastal segments. (Kirezci et al., 2020; Paprotny et al., 2016; Vafeidis et al., 2008; Vousdoukas et al., 2016). The spatial extent in large-scale coastal flood hazard assessment does not allow running simulations for the entire domain so far (Vousdoukas et al., 2016). The division in segments can be uniform over the total shoreline (Vousdoukas et al., 2016) or of variable length (Vafeidis et al., 2008). Vafeidis et al. (2008) used a segmentation model that defines segments with more or less uniform values along their length. This can be based on longshore variation of various parameters related to coastal geomorphology, population density and administrative boundaries.

For the assessment of the interaction with natural and artificial defences, protection levels of the coastal segments are required. The availability of information about flood protection standards can significantly impact the model results (Paprotny et al., 2019). The protection standards are commonly implemented as nominal protection levels in terms of return periods (Scussolini et al., 2016) or as heights above mean sea level, linking return periods with ESLs including tides (Vousdoukas et al., 2016). In the former case, the standards are either design levels of actual defences, legal requirements in a given area or estimates based on expected annual damages (Paprotny et al., 2019; Tiggeloven et al., 2020). However, in multiple studies the presence of coastal protection is not included in the analysis (Jongman et al., 2012; Kirezci et al., 2020; Muis et al., 2016).

CFR component 3

In case natural or artificial coastal boundaries are exceeded by the extreme sea level, the corresponding flood hazard will propagate further inland. How the flood hazard propagates inward in a simulation depends on the modelling type. However, in all cases a digital elevation model (DEM) is required as a basis for elevation of the hinterland. The accuracy of the DEM can have significant impact in the results of the assessment (Hinkel et al., 2021; Paprotny et al., 2019; Vousdoukas et al., 2018a; Vousdoukas et al., 2016). For the propagation of the flood hazard inward, both the static Bathub approach as well as process-based hydrodynamic modelling approach can be applied.

Typical model outcomes

The results gathered through the use of coastal inundation models are typically on the characteristics of the flood extent such as flooded area and inundation depth.

One of the main outcomes of coastal inundation models is the flood extent. This can be presented as a total flooded area in km² over the complete spatial domain as an area per country (Vousdoukas et al., 2016). Furthermore, normalization per coastline length can be performed to present the flooded area per unit length of coastline (Kirezci et al., 2020).

Assumptions, uncertainties and limitations

Large-scale coastal flood hazard assessments are available to a limited extent and contain several underlying assumptions, uncertainties and limitations. Within previously performed research, these are inventoried and their effects on the model outcomes are studied. In general, the assessments are based on lower-resolution DEMs and exposure data. Next to that, the hydrology and hydraulics, as well as flood damage processes are abstract conceptualizations of physical processes. The relative contribution of uncertainty factors is site specific and not generally valid. The data available and methods used also play a role in this (Vousdoukas et al., 2018a). However, even when high quality data is available, a trade-off between data resolution used, model complexity and computational power is necessary at present (Vousdoukas et al., 2016). In this section, the most important assumptions, uncertainties and limitations are described in detail.

1. Data scarcity

In general, data scarcity forms a generic problem for global scale coastal analysis. This includes the resolution, coverage parameter availability and data sources (Vafeidis et al., 2008). Since the accuracy of broad-scale assessments is impacted by these data sources, development of these systems continues. Appropriate and reliable information forms an important part in this (Vafeidis et al., 2008). Furthermore, the data should be well organised, planned and in coherent coastal databases to be useful. Vafeidis et al. (2008) named the following commonly encountered limitations:

1. Different data formats;
2. Incompatible projections between datasets;
3. High costs for integrating nondigital datasets;
4. Lack of metadata;
5. Incomplete spatial coverage (Vafeidis et al., 2008).

These commonly encountered limitations arise in different types of data used in coastal hazard assessments, such as elevation data and flood protection data.

2. DEM resolution

The used digital elevation model (DEM) is crucial for inundation modelling. Sub 10 meter resolution Lidar data is recommended for reliable results (Vousdoukas et al., 2016). However, such datasets are not commonly available on larger scales and such resolution is furthermore too computationally expensive. Multiple sources name the resolution of the DEM as one of the main underlying uncertainties and limitations in global coastal flood hazard modelling, irrespective of the type of inundation model applied (Hinkel et al., 2021; Paprotny et al., 2019; Vousdoukas et al., 2018a; Vousdoukas et al., 2016). Global DEMs affect the quality of large-scale assessments by (Vousdoukas et al., 2018a):

1. Simplifying the terrain relief;
2. Adding systematic bias;
3. Not resolving natural or artificial coastal protection elements (Vousdoukas et al., 2018a).

However, even if the DEMs were of better quality, the previously mentioned trade-off between DEM resolution and computational costs remains. Vousdoukas et al. (2018a) stated that the computational cost of the analysis increases exponentially with DEM resolution.

3. Protection levels

Another major uncertainty within large-scale coastal flood hazard assessments arises from protection levels and human adaptation (Hinkel et al., 2021; Paprotny et al., 2019; Vousdoukas et al.,

2018a). For the baseline (current) scenarios, this is mainly due to scarcity of detailed information about flood protection. Detailed information (e.g. dimensions and condition) about natural (dunes, cliffs, beaches) and artificial (sea walls, dikes) coastlines is commonly only available from local studies (Paprotny et al., 2019). Information such as their nominal protection level, probability of failure and maintenance level are not systematically available at large spatial scales (Hinkel et al., 2021). On larger scales, efforts are taking place for coastal regions (e.g. the FLOPROS database by (Scussolini et al., 2016) as well, although it remains sparse and heterogeneous (Vousdoukas et al., 2018a). As Vousdoukas et al. (2018a) stated, existing datasets suffer from multiple sources of errors, such as:

1. The fact that protection standards are often reported as return periods and conversion in ESLs can include artefacts, among others, from the components considered, the extreme value analysis, and model errors (Vousdoukas et al., 2018c);
2. Most datasets provide one value for extensive regions covering several kilometers along which protection levels can vary substantially;
3. There is no centralized system to collect and update information on available coastal protection in most countries, not to mention at continental or global scale. (Vousdoukas et al., 2018a)

In some studies, protection standards are not included in the analysis. This could lead to bias of up to a factor 1300 in the year 2100 (Hinkel et al., 2021). Next to that, it is misleading since it is known that extensive defence systems exist, especially in developed and well populated coastal locations around the world (Oppenheimer & Glavovic, 2019). Furthermore, just using a nominal protection level also has some pitfalls. This includes e.g. that only overtopping of flood protection is taken into account. Besides, coastal segments are not completely independent from each other i.e. if one segment fails, multiple sections of the hinterland can be inundated (Hinkel et al., 2021). Large-scale coastal flood hazard assessments so far have either (Hinkel et al., 2021):

1. Focused on flood exposure and ignored coastal protection (Hanson et al., 2011);
2. Only considered overflow but not breaching (Vousdoukas et al., 2018b);
3. Only considered breaching assuming that once an ESL exceeds defense heights, defenses breach and fail completely (Diaz, 2016; Hinkel et al., 2014; Lincke & Hinkel, 2018; Tamura et al., 2019), or a combination of the latter two (Hallegatte et al., 2013; Hinkel et al., 2021).

4. *Extreme sea levels*

The extreme sea levels (ESLs) used within coastal flood hazard assessments differ per study. The components contributing to this ESL, are mentioned in section 1.1.2. Some of the main improvements in the extreme sea levels included in coastal flood hazard assessments include (Vousdoukas et al., 2016):

1. Considering the contribution of wave run-up to the TWLs (Perini et al., 2016; Serafin & Ruggiero, 2014);
2. Applying a multivariate approach for the extreme value statistics (Corbella & Stretch, 2013; Gouldby et al., 2014; Hawkes et al., 2002);
3. Taking into account all the wave-related processes contributing to coastal flooding (i.e., erosion, overwash and breaching (Matias et al., 2008; McCall et al., 2010; Vousdoukas et al., 2016).

Vousdoukas et al. (2016) studied the impact on the coastal flood hazard of including waves to the ESLs. Results showed that, omitting wave contribution resulted in a 60% underestimation of the flooded area when using the LISFLOOD-AC inundation approach. However, the wave setup only contributed for 5% to the global area inundated by 2100 while using a planar Bathtub approach (Kirezci et al., 2020). Furthermore, uncertainty arises from the interaction between mean sea-levels, storm surges, tides and waves (Hinkel et al., 2021; Vousdoukas et al., 2018a). Related to the forcing water level, part of the inaccuracy in large-scale assessments might stem from neglecting the influence of river discharge (Paprotny et al., 2019).

Related to the components contributing to the total water level, is the uncertainty due to the extreme value analysis (EVA) method applied (Mentaschi et al., 2016; Wahl et al., 2017). For future coastal flood hazard assessments, forcing water levels with a return period of e.g. 100 or

1000 years are used. However, statistical extrapolation of the data has to be applied since no data is available for such time frames. This results in large confidence limits of the estimates. The type of extreme value analysis can have a major impact in the estimates of the extremes (Kirezci et al., 2020).

5. Future development

While present uncertainties are already influencing the coastal flood risk assessment, future developments will further increase the uncertainties. This relates to socioeconomic development, climate change and sea level rise, future exposure and adaptation scenarios. Population growth, urbanization, land use change and coastward migration all have an impact on the exposure and vulnerability to coastal flood risk. Furthermore, technological developments in e.g. early warning systems, health care and building resistance have an impact on the future vulnerability of societies to coastal flood risk (Hinkel et al., 2021). Differences in climate scenarios (e.g. RCP4.5 vs RCP8.5) can be very large. It is even possible that opposite trends are indicated (Paprotny et al., 2019). Related to this, differences in the expected greenhouse gas emissions and corresponding climate change projections increase the uncertainty in the future coastal flood risk assessment (Hinkel et al., 2021; Vousdoukas et al., 2018a).

6. Inundation modelling techniques

Several types of inundation modelling techniques have been applied in previously performed large-scale coastal flood hazard assessments. Within these modelling techniques, the most characteristic difference is between static and dynamic models. However, both have inherent limitations and uncertainties. On local scales, process-based (dynamical) inundation models are generally applied, but on larger scales these models are too computationally expensive and require high resolution topographic data. The computationally efficient static models can overestimate the potential flood extent, within local studies, by a factor 0.5-2 in flatter terrains, when overtopping is the main flooding process involved (Breilh et al., 2013; Gallien, 2016; Ramirez et al., 2016; Seenath et al., 2016). However, at large scale the limitations of the static approach are hardly assessed (Hinkel et al., 2021). Vousdoukas et al. (2016) performed a large scale comparison study between a static (Bathtub) approach and a process-based dynamic (LISFLOOD-AC) model at European scale and results showed that the static approach estimates the flood extent with a factor 1.56 larger than the dynamic model for the whole of Europe. However, the dynamic models do not necessarily provide better results. These models need to be calibrated to regional circumstances, which is not straightforward in broad scale studies (Hinkel et al., 2021).

Inundation modelling techniques

As Hinkel et al. (2021) stated: "*The propagation of mean and extreme sea-levels into the hinterland causing coastal flooding is shaped by how sea levels interact with the coastal profile including the natural (e.g., dunes) and artificial (e.g., dikes, seawalls) flood barriers in place.*" To simulate this interaction, several inundation modelling techniques can be applied. These range from simple, static approaches to complete physically process-based models. However, on a global scale a trade-off between model complexity and resolution with computational intensity is required (Hinkel et al., 2021). Therefore, intermediate approaches have been developed.

Vousdoukas et al. (2016) investigated the developments in large scale coastal flood mapping and identified the so-far applied approaches. The intermediate solutions differ in the way they account for mass conservation (Breilh et al., 2013), aspects of flooding hydrodynamics (Dottori et al., 2018) or the presence of obstacles (Perini et al., 2016; Sekovski et al., 2015). Furthermore, Bates et al. (2010) developed a dynamic, reduced complexity model LISFLOOD-FP, originally developed for river flow processes. Although it was originally developed for river flow processes, its application in coastal assessment, referred to as LISFLOOD-AC, is proven to be reliable as well. Also on larger scales, their potential application to coastal flooding is promising (Vousdoukas et al., 2016).

1.2 Problem statement

The process-based numerical model LISFLOOD-AC used for coastal flood inundation estimates on a global scale is a relatively computationally expensive model. The commonly used Bathtub approach does not have this limitation, although this model can overestimate the flood magnitude (Vousdoukas et al., 2016). Therefore, rigorous assessment of the additional error being made in the assessment of coastal flood hazard by using this latter, simplified approach, is required. With this assessment, it can be investigated whether the computational time of models can be reduced without compromising on quality of results.

Currently, the assessment of coastal flood hazard beyond regional and national scales is scarce (Paprotny et al., 2019; Vousdoukas et al., 2018a; Vousdoukas et al., 2016). Besides, the existing large scale assessments are based on the static (Bathtub) approach (Hinkel et al., 2014; Hinkel et al., 2010). The underlying uncertainty, structural limitations and scaling effects are rather unknown (Vousdoukas et al., 2018a). Simultaneously, a significant increase in coastal flood hazard is expected due to changes in storm patterns and sea level rise (Church & Gregory, 2019; Forzieri et al., 2016). For these reasons, coastal flood risk assessment at a large scale is needed, taking into account climate- and socioeconomic changes.

1.3 Scope

During the research project the spatial focus is on the global domain. More specifically, the entire stretch of coastline around the world is under study. Within this spatial scope, the inundation models give results as a magnitude of flooding which contains its landward extent and its inundation depth for different return periods of extreme sea levels.

The large scale coastal flood hazard assessments will help policy makers and engineers in decision making to develop adaptive strategies for reduction of coastal flood risk (Scussolini et al., 2016). Within this research project two global coastal flooding models will be assessed and compared; the static Bathtub approach and the process-based LISFLOOD-AC model. Comparing both models for the baseline period 1980-2014 is the main priority during this research project. Identifying differences in estimated flood extent is the main task in achieving this goal.

1.4 Objective and research questions

The objective of this study is to investigate global inundation estimations from the Bathtub approach, and to critically compare the approach and results to the outcomes of the more detailed, global scale process-based model LISFLOOD-AC.

Of first priority is the investigation of differences in flood extent and the identification of why these arise. In this, the focus will be based on the baseline model results.

Eventually, this research project will help in extending and producing knowledge of the limitations, uncertainties and applicability of global coastal flooding models. Hereby taking into account a compromise between model complexity, data requirements vs. availability and constraints in computational power (Vousdoukas et al., 2016).

To achieve the objective of the research, the main research question is structured as follows:

How does the Bathtub modelling approach compare to the LISFLOOD-AC model in terms of applicability to global scale coastal flood hazard estimation?

To answer the main research question it is split up in three subquestions.

1. How does the Bathtub approach compare to the LISFLOOD-AC model in estimations of the flood extent based on administrative boundaries?
2. What are the differences in estimated flood extent based on different coastal typologies and why are these observed?
3. What are the differences in estimated flood extent based on different coastal terrain types and why are these observed?

1.5 Thesis outline

The structure of this thesis is as follows: First a literature review is presented to provide essential background information on the topic of coastal flood risk assessment and modelling, thereafter the model set up of the two models under study are outlined, subsequently the methodology adopted to answer the research questions is described. In chapter 4 the results are presented for the subquestions. Based on the preceding chapters, a discussion and conclusion are finally established.

2 | Coastal flooding models under study

Although the Bathtub approach and the LISFLOOD-AC model are not build and run during this research project, their set up and the input data used are of importance for the context of the model results. In this chapter, both modeling approaches are outlined in detail and the input data used is presented. The first part describes the two modelling approaches after which the focus is on the model set-up and input data in this research project. The chapter ends with a comparison of the two methods.

2.1 Bathtub approach

The static Bathtub approach is a commonly applied, simple method to assess the coastal flood hazard. In this approach, the coastal zone is represented as a 'bathtub' i.e. all areas with elevation lower than the forcing water level will be inundated if they are hydraulically connected with the sea (Paprotny et al., 2019; Vousdoukas et al., 2018a). The different applications of the Bathtub approach are displayed in Figure 2.1. The one applied in this study is the application that considers adjacent as well as diagonally, hydraulically connected cells (8-connected). In other words, a cell would be flooded if it is below the extreme sea level and connected to an adjacent or diagonal flooded cell or open water (Poulter & Halpin, 2008). The inundation depth is then computed as the difference between the land elevation of the cell and the forcing water level (Vousdoukas et al., 2018a). This static approach is the simplest applicable method and comes with relatively low computational costs and can be applied in a GIS (Geographic Information System) environment (Seenath et al., 2016).

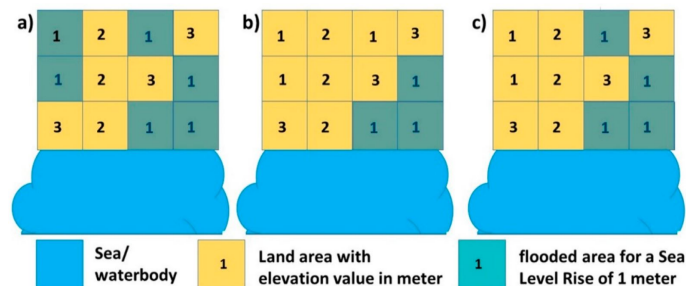


Figure 2.1: Different Bathtub approaches. In a) no hydraulic connectivity is considered, in b) hydraulic connectivity is considered for adjacent cells (4-side connectivity) and in c) also hydraulic connectivity of diagonal cells is considered (8-side connectivity). From Yunus et al. (2016).

2.2 LISFLOOD-AC model

The reduced complexity model LISFLOOD-AC is part of the LISFLOOD-FP model by Bates and De Roo (2000). This LISFLOOD-FP model was originally developed to analyse river flooding and consists of a 1-dimensional kinematic wave approximation for channel flow and a two-dimensional diffusion wave representation of floodplain flow. To lower the computational costs whereby making flood hazard assessment on larger scales possible, the LISFLOOD-AC model has been developed by Bates et al. (2010). The LISFLOOD-AC model has a 1-dimensional inertial (so advection is not considered) model where x and y directions are decoupled. These decoupled directions are

then combined to represent a 2-dimensional simulation over a raster grid (Vousdoukas et al., 2016).

The LISFLOOD-AC model makes use of the Shallow Water equations. The derivation of the governing equations therefore starts with the momentum equation from the one-dimensional Shallow Water (or Saint-Venant) equations:

$$\underbrace{\frac{\partial Q}{\partial t}}_{\text{acceleration}} + \underbrace{\frac{\partial}{\partial x} \left[\frac{Q^2}{A} \right]}_{\text{advection}} + \underbrace{\frac{gA\partial(h+z)}{\partial x}}_{\text{water slope}} + \underbrace{\frac{gn^2Q^2}{R^{4/3}A}}_{\text{friction slope}} = 0 \quad (2.1)$$

, where Q is the discharge, A is the flow cross section area, g is the acceleration due to gravity, h is the flow depth, z is the bed elevation, n is the Manning's friction coefficient and R is the hydraulic radius.

The flows advection is relatively unimportant for many floodplains (Hunter et al., 2007). Since the advection (convective acceleration) terms are therefore negligible compared to the other terms, advection is not considered. Furthermore, in the derivation a rectangular channel is assumed and the hydraulic radius is approximated by the flow depth (applicable for wide, shallow flows). This ends up in the following equations, decoupled in x- and y-direction:

$$\frac{\partial q_x}{\partial t} + gh \frac{\partial(h+z)}{\partial x} + \frac{gn^2||\mathbf{q}||q_x}{h^{7/3}} = 0 \quad (2.2)$$

$$\frac{\partial q_y}{\partial t} + gh \frac{\partial(h+z)}{\partial y} + \frac{gn^2||\mathbf{q}||q_y}{h^{7/3}} = 0 \quad (2.3)$$

, where q represents the flow per unit width.

Furthermore, a continuity equation, in the form of a mass-balance, is included in the model (equation 2.4). This relates flow into a cell and its change in volume.

$$\frac{\partial h}{\partial t} + \frac{\partial q_x}{\partial x} + \frac{\partial q_y}{\partial y} = 0 \quad (2.4)$$

The potential flooding area is discretized as a fine spatial resolution regular grid. Each cell on the grid then represents a storage area for which the mass balance (represented by the continuity equation) is updated at every time step. This mass balance is updated according to the fluxes of water into and out of each cell.

Numerical stability for the shallow wave propagation represented in LISFLOOD-AC is dependent on the Courant-Freidrichs-Lewy condition. Therefore, the LISFLOOD-AC model is able to run at bigger time steps, since the stable time step (for numerical stability) scales with $1/\Delta x$ instead of $(1/\Delta x)^2$ applicable to diffusive storage cell models like LISFLOOD-FP (Bates et al., 2010).

The maximum stable time steps for diffusive storage cell models decreases rapidly with resolution due to the squared grid resolution divided by four (Hunter et al., 2005), as can be seen in equation 2.5.

$$\Delta t = \frac{\Delta x^2}{4} \left(\frac{2n}{(h_{flow}^t)^{5/3}} \left| \frac{\Delta(h^t+z)}{\Delta x} \right|^{1/2} \right) \quad (2.5)$$

, where Δx is the cell size, h_{flow} is the depth between cells through which water can flow, h is the cell water depth and n is Manning's roughness coefficient.

To have a stable model at longer time steps, a full shallow water model (e.g. Mignot et al. (2006)) has potential. However, this will require more computational effort per time step (Neal et al., 2011). Therefore, Bates et al. (2010) developed an intermediate solution: the LISFLOOD-AC model. The diffusion and inertial terms of the 1-dimensional shallow water equation are considered in this approach. In this way, the stable time step can be increased while the additional physical representation is minimized. This 1-dimensional equation is solved for both the decoupled x and y direction on every face of a 2-dimensional grid cell, which provides a 2-dimensional solution. The maximum time step to ensure numerical stability for this model is presented by equation 2.6:

$$\Delta t_{max} = \alpha \frac{\Delta x}{\sqrt{gh_t}} \quad (2.6)$$

, where α is a stability coefficient that ranges from 0.2 to 0.7 for most floodplains and g is the acceleration due to gravity.

At every time step, the mass balance is updated through the use of the continuity equation (Bates & De Roo, 2000):

$$h_{i,j}^{t+\Delta t} = h_{i,j}^t + \Delta t \frac{Q_{xi,j-1}^t - Q_{xi,j}^t + Q_{yi,j-1}^t - Q_{yi,j}^t}{\Delta x^2} \quad (2.7)$$

, where Q is the flow between cells, calculated at the cell faces using a centred difference scheme decoupled in x or y directions, h is the water depth at the centre of each cell and Δx is the cell width, while i and j are cell spatial indices.

Since the LISFLOOD-AC formulation only makes use of the inertial terms of the shallow water equation, the calculation of the flux between cells includes the flux from the previous time step and a term for acceleration due to gravity. This gives equation 2.8

$$Q^t = \frac{q^t - gh_{flow}^t \Delta t \frac{\Delta(h^t+z)}{\Delta x}}{\left(1 + gh_{flow}^t \Delta t n^2 |q^{t-\Delta t}| / \left(h_{flow}^t\right)^{10/3}\right)} \Delta x \quad (2.8)$$

, where z is the bed elevation, n is Manning's roughness coefficient and h_{flow} is the depth between cells through which water can flow.

Overall, the LISFLOOD-AC model is a less computationally expensive model compared to full shallow-water models (like Mignot et al. (2006)), while providing results of similar accuracy compared to more complex models, both in terms of flow velocity and water depths (Neal et al., 2011).

2.3 Model set up and input data

In this section the structure of the models applied as well as the input data used in the simulations is addressed. This overlaps to a large extent for the Bathtub approach and the LISFLOOD-AC model. However, for the application of the LISFLOOD-AC model, additional input is required compared to the Bathtub approach. This is a result of the more complex nature of the LISFLOOD-AC model.

2.3.1 Spatial domain and coastal segments

The spatial domain of this study involves the entire stretch of coastline around the World. Model results of both the Bathtub approach and the LISFLOOD-AC model are made available between -180 to 180 degrees longitude and -60 to 80 degrees latitude. Antarctica and Greenland are not included in the model results.

Since both models are run on a global scale, discretization into coastal segments is necessary for computational reasons. Therefore, the entire global coastline was split up in coastal segments of 100 km. However, the exact length of each segment depends somewhat on the resolution of the coastline. For all these segments, an inland extent of 100 kilometers is considered in the model runs.

2.3.2 Model scenarios

The scenarios run are determined by the different ESLs from the baseline (1980-2014) reference period, resulting in six different model scenarios (Table 2.1). These will be referred to as 'baseline return periods' since 'scenarios' might induce confusion with climate change scenarios.

Table 2.1: The six different model scenarios included, referred to as baseline return periods. These are determined by the different ESLs from the baseline reference period 1980-2014.

Return period [yr]	Reference period	Baseline period (1980-2014)
5		Baseline 5-year event
10		Baseline 10-year event
20		Baseline 20-year event
50		Baseline 50-year event
100		Baseline 100-year event
200		Baseline 200-year event

2.3.3 Extreme sea levels

A complete description of how the extreme sea levels (ESLs) are established is presented in Voudoukas et al. (2018c). The most important aspects are briefly described in this paragraph. The ESLs used in the global flooding simulations are estimated for points every 100 kilometer along the coastline. These ESLs consist of a tidal, storm surge and wave setup component.

$$ESL = MSL + \eta_{tide} + \eta_{CE} \quad (2.9)$$

, with MSL the mean sea level, η_{tide} the high tide water level and η_{CE} the water level fluctuations due to climate extremes (waves set up and storm surge by wind)

To assign an ESL estimate for every source point, a global dataset for extreme sea levels is established. For the tidal component of the ESL, time series of tidal elevation were gathered from the FES2014 model of Aviso, France. Furthermore, for the storm surge component a hindcast run with Delft3D-Flow is applied for extreme storm surge levels, with atmospheric pressure and wind fields. These wind fields were obtained from time series of significant wave height from the ERA-interim database. Time series of the significant wave height have been established using the third generation spectral wave model WW3. The contribution of the storm surge and significant wave height to the ESLs is determined with the following equation:

$$\eta_{W-SS} = SSL + 0.2\dot{H}_s \quad (2.10)$$

, with H_s the offshore significant wave height.

This 0.2 times the significant wave height is considered to be a reasonable approximation of the wave setup. With wave setup being the water level elevation due to wave shoaling and breaking of waves near the coast (US Army Corps of Engineers, 2002).

The ESLs used within the two models differ since the LISFLOOD-AC model contains a temporal component while the Bathtub approach does not. This time-dependent component of the ESL is defined by performing a Monte-Carlo analysis for high tides. In this analysis, probability density functions (PDFs) for sea level rise, storm surge contribution and wave set up are included. Similarly, the tidal component has its own PDF corresponding to a spring tide, neap tide or something in between. These PDFs all express an uncertainty. With the Monte Carlo simulations, a synthetic triangular hydrograph is established. Subsequently, all source points along the coastline have a storm event at the same moment. This estimate event is fitted as a duration of the peak of the storm at ESL at each location.

An example map of the global median present-day 100-year ESL is presented in Figure 2.2.

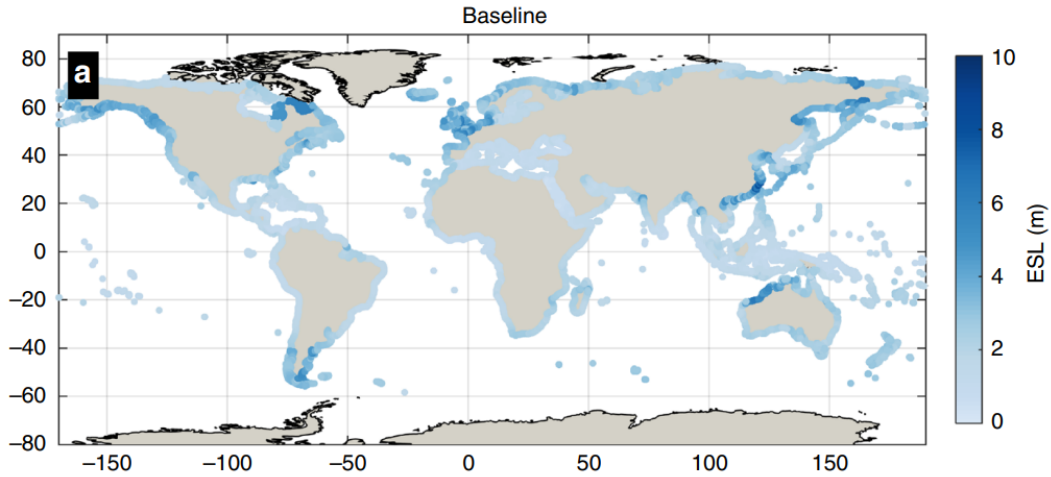


Figure 2.2: Global median present-day 100-year ESL, from Vousdoukas et al. (2018c).

2.3.4 Digital elevation model

For the estimation of the coastal flooding, both the Bathtub approach and the LISFLOOD-AC model require an elevation model. In both computations, a DEM by Copernicus is used. This digital elevation model represents the Earth’s surface, including buildings, infrastructure and vegetation (AIRBUS, 2020). The GLO-90 DEM is the instance which is used in both models, containing a 90m resolution and a global geographical extent.

2.3.5 Flood protection data

Through a collaboration between IHE Delft Institute for Water Education and the JRC of the European Commission, protection standards for the World’s coastline have been established. The protection standards are represented as nominal protection levels in terms of return periods. These protection standards are estimated based on urbanization, population density and the presence of ports and airports, combined with income classes. The range of possible protection standards is set from once per year to 1-in-100 years. An overview of the corresponding protection standards is presented in Table 2.2. When two conditions are satisfied, the maximum return period is used.

Table 2.2: Protection standard per criterion and income class.

Criterion	Income class (GDP per capita [USD/year])				
	0-1000	1000-4000	4000-12000	12000-40000	40000>
Urbanization: 10% artificial land or popDensity>500 people/km ²	1	2	5	10	30
Large Port	10	10	10	50	50
Small port	2	2	10	10	10
Airport	2	5	10	30	100

However, the values from the table are overwritten for Belgium, China, the Netherlands and the USA since detailed datasets of protection levels for these regions were available. Thus the range of protection levels adopted in this study spans between 1-10000 year return periods.

The required data for the criteria are established as follows:

- The income classes used, were gathered from the World Bank classification (‘New World Bank country classifications by income level: 2020-2021’, n.d.). Although an extra class of GDPcapita>40000 USD/year is included;
- Small and large ports were established from WFPGeoNode (‘Global Ports — WFP GeoNode’, n.d.) and from The Humanitarian Data Exchange (‘Global ports (WFP SDI-T - Logistics Database) - Humanitarian Data Exchange’, n.d.);
- The airport data was gathered from The World Bank (‘Global Airports | Development Data Hub’, n.d.) and from Partrow (‘The Global Airport Database - By Arash Partow’, n.d.);

- The global land use data, used for urbanization information, is established from a dataset by the European Space Agency ('ESA Data User Element', n.d.);
- Global gridded population data was gathered from the Socioeconomic Data and Application Center (SEDAC) of NASA ('Data » Gridded Population of the World (GPW), v4 | SEDAC', n.d.);
- Global gridded Gross Domestic Product (GDP) data was established from (Kummu et al., 2018).

Overall, the collaboration between IHE and the JRC resulted in a dataset for protection level standards along the World's coastline in which available protection standard data was combined with criterion based protection standards. A total of 38127 protection level points (for longitude and latitude values) are present in the dataset (Figure 2.3).

The protection levels are included in both models by not allowing any inundation if the return period of the total water level is lower than the flood protection level for a specific coastal segment.

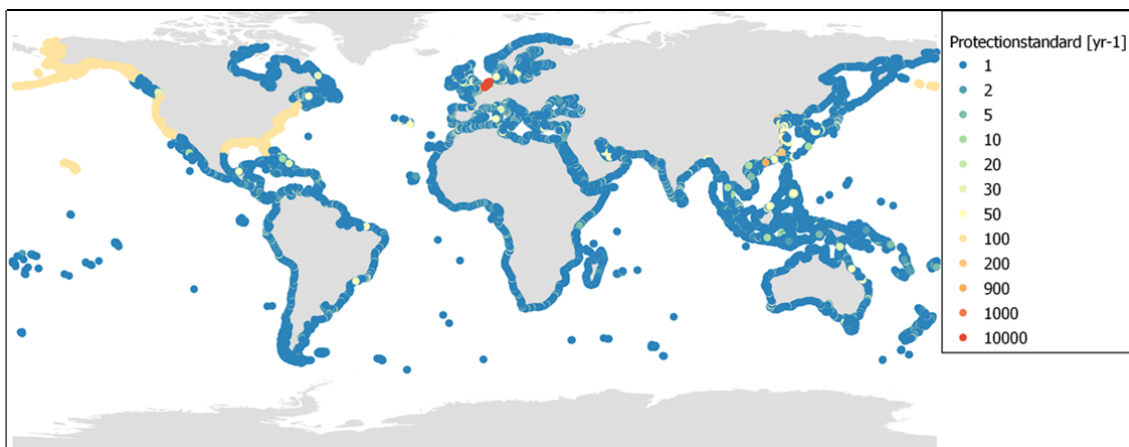


Figure 2.3: Global overview of flood protection standards included. With the range of protection levels spanning between 1-10000 year return periods.

2.3.6 Synthetic hydrograph

Since the LISFLOOD-AC model has a temporal component, the forcing water level changes over time as well. This is enabled by the integration of a synthetic hydrograph, representing a relationship between the ESL and a time-component. In the LISFLOOD-AC model a triangular synthetic hydrograph is considered (Figure 2.4).

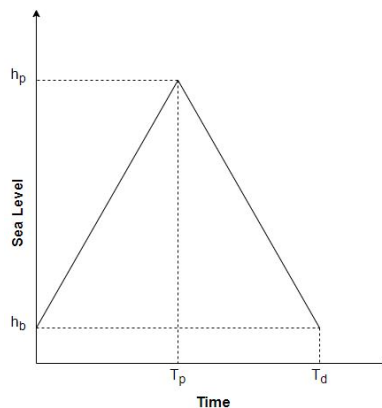


Figure 2.4: Triangular synthetic hydrograph. With h_b being the base (mean) sea level, h_p being the extreme sea level (ESL), T_p being the time to ESL and T_d the duration of the hydrograph.

2.3.7 Hydraulic roughness values

In the LISFLOOD-AC model, the flood propagation over land is influenced by the surface roughness. To integrate this in the model, hydraulic roughness values are established from the GlobCover 2009 from ESA (the European Space Agency) (Bontemps et al., 2011). This land cover map contains 22 land cover classes on a global geographical extent. These classes are equal to the classes defined by the Land Cover Classification System (LCCS) of the United Nations (UN). The land use classes of GlobCover have been derived by an automatic and regionally-tuned classification of a time series of global MERIS FR mosaics ('ESA Data User Element', n.d.). A conversion table is used to couple the land cover classes to a specific Manning's roughness value, which is used in the LISFLOOD-AC computation.

2.4 Comparison of both modelling approaches

The characteristics of the Bathtub approach and the LISFLOOD-AC model are different to a large extent. Where the Bathtub approach is static, without a temporal component and not including physical processes, the LISFLOOD-AC model is dynamic and physically based. This makes the Bathtub approach more simple to apply and simultaneously providing results faster.

Vousdoukas et al. (2016) and Ramirez et al. (2016) compared the Bathtub approach with a dynamic approach and both concluded that the static Bathtub approach is overestimating the flood hazard area, to a degree depending on the type of coast. Vousdoukas et al. (2016) stated that: "*low-lying vicinities of estuaries and deltas are particularly prone to errors compared with steeper coasts.*" Flood extents as estimated by the Bathtub approach are about 1.6 times larger than these from the LISFLOOD-AC model, resulting from the comparison on a European scale by Vousdoukas et al. (2016).

Although the LISFLOOD-AC model produced more accurate results in prior, restricted research, the Bathtub approach is still frequently used due to the difference in processing time and complexity of the LISFLOOD-AC model. The ratio of computational time between the LISFLOOD-AC model and the Bathtub approach is 1 to 10 respectively. The time it takes to run the LISFLOOD-AC model, including making sure that everything runs properly, is in the order of days.

The LISFLOOD-AC model is less easily applicable due to the difference in complexity and implementation. While the Bathtub approach can just be run in a GIS environment, the LISFLOOD-AC model requires Fortran coding. This results in a different set of skills required to be able to run a simulation using the LISFLOOD-AC model.

2.5 Description of model outcomes

A global dataset with model outcomes from the LISFLOOD-AC model as well as for a Bathtub modelling approach is used. The reference period 1980-2014 is used as the baseline period in this study. For this baseline period, six return periods of extreme sea levels are taken into account: once per 5, 10, 20, 50, 100 and 200 years respectively. This makes a total of 6 scenarios. These model outcomes are presented by a collaboration from IHE Delft Institute for Water Education and the JRC. The model outcomes used include the flood extent with a corresponding inundation depth.

The model outcomes for both models are available as tiles (.mat files) that cover 100 kilometer of shoreline and 100 kilometer inland extent. These tile files are structured as georeferenced arrays, with cell values representing the floodwater depth in meters. The model results are available for a geographical extent of -180 to 180 degrees longitude and -60 to 80 degrees latitude. Greenland and Antarctica are not included in the results. The resolution of the flooding data is equal to the resolution of the underlying DEM, which is the 90m Copernicus DEM. A total of around 700 tile files are available for every scenario.

3 | Methodology

The methodology to gather answers to the research questions presented in section 1.4 is outlined in this chapter. This includes the description of the data used, data post-processing and the methods applied.

3.1 Flood data post-processing

The output data of both the Bathtub approach and the LISFLOOD-AC model are post-processed to be able to determine the flooded area and the fit metrics. A description of the output data of by both models is presented in Section 2.5. The processing steps are similar for both models and are outlined in the following paragraphs.

3.1.1 Matlab to GeoTIFF files

The model results are transformed from Matlab tiles to GeoTIFF files to make comparison using geographical information systems (GIS) possible. This facilitates visualization of the flooded area estimates and subdivision based on geometrical boundaries. Due to the irregular shape of the coastline, the model results overlap in some regions. Furthermore, the .mat files are transformed to GeoTIFF files of 5 by 5 degrees and therefore include multiple .mat files per GeoTIFF file (Figure 3.1). To come to one GeoTIFF file with the model results for a 5 by 5 degree geographical extent, the maximum flood depth of overlapping cells is taken. This results in GeoTIFF files of 6001 by 6001 pixels, resulting in a resolution of 8.3×10^{-4} degrees, which translates to a resolution of 90 m at the equator and 55 m at 70 degrees longitude. All files are in the coordinate reference system EPSG:4326 on the WGS84 reference ellipsoid.

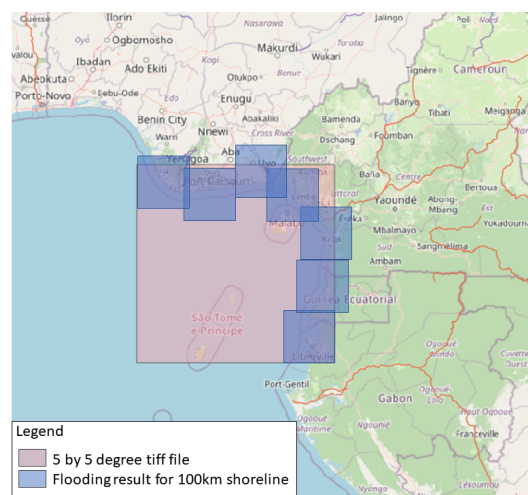


Figure 3.1: Converting flooding results for 100km of shoreline to a 5 by 5 degree GeoTIFF file. With in pink the GeoTIFF file combining the flooding results per 100km of shoreline as represented by the blue boxes

3.1.2 Inundation of surface water

The raw flooding results show inundation of water bodies i.e. inundation of lakes and rivers. To estimate the flooded area, this inundation of surface water is removed from the data (Figure 3.2). The Global Surface Water Explorer (GSWE) data from the JRC is used for this (Pekel et al., 2016). More specifically, the presence of surface water over the period 1984-2020 is used to cut out the inundation of permanent water bodies. The data present in the GSWE is established from Landsat satellite imagery and is available in a resolution of 30 meters. To remove permanent water bodies from the global flooding estimates of the Bathtub approach and the LISFLOOD-AC model, a threshold of 80% occurrence of water over the period 1984-2020 is applied. This will minimize the removal of floodplain inundation in the results while making sure that the permanent water bodies (i.e. lakes and rivers) are removed. This procedure has previously been applied by Aerts et al. (2020).

The GSWE raster was cut in 5-by-5-degree files using GDAL translate, which is a tool to convert raster data between different formats ('GDAL — GDAL documentation', n.d.). This ensures that the same extent is present for the GSWE files as the model outcomes. Subsequently, the inundation of permanent water bodies is removed from the flooding estimates, by reclassifying the occurrence data to 0 or 1 whether the threshold value of 80% is exceeded or not. This was performed using the GDAL calc tool, a command line raster calculator. With this tool the value per pixel (the percentage of occurrence of surface water) is evaluated and changed to 0 if it is equal or higher than 80% and to 1 if it is lower than 80%. Subsequently, the resolution of the reclassified GSWE GeoTIFF is set to the same resolution of the model outcomes ($8.3 \cdot 10^{-4}$ degrees) using GDAL warp, an image reprojection tool. Finally, the reclassified GeoTIFF files are multiplied with the flooding estimates from the Bathtub approach and the LISFLOOD-AC model using gdal calc. This assures that water bodies are removed from the data by multiplying them with a value of zero (from the reclassified GeoTIFF).

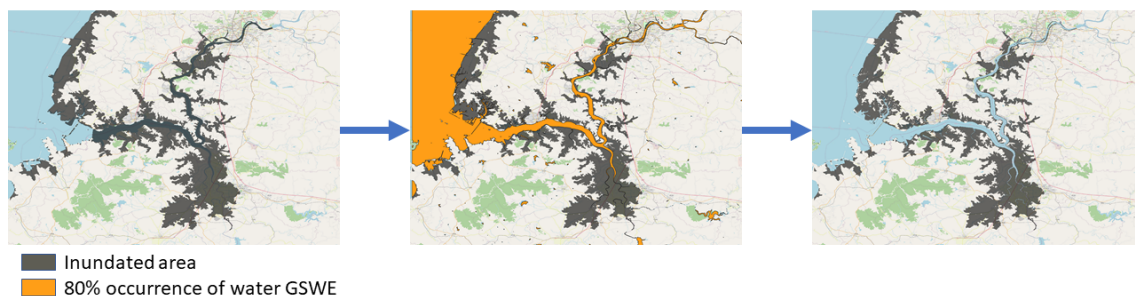


Figure 3.2: Removing inundation of water bodies by using the GSWE (Global Surface Water Explorer) reclassified data: Example of a region in China. From left to right: original flooding data in dark; reclassified GSWE in orange representing surface water with an occurrence of 80% over the period 1984-2020; and reclassified GSWE cut out of flooding data and therefore removing surface water from the model output.

3.1.3 Reclassifying and area determination

At first, the GeoTIFF files including the flooding results are reclassified to GeoTIFF files containing a value of 1 if a cell is flooded and 0 if it is not. This is performed the same way as for the GSWE reclassification (Section 3.1.2). In this, every cell with a flood depth bigger than zero is classified as flooded. Furthermore, the flooding results are in the coordinate reference system EPSG:4326 on the WGS84 reference ellipsoid. This reference system is in units of degrees longitude and latitude. To determine the flood extent in square kilometers, a GeoTIFF file containing the area per cell is determined for every 5 by 5 degrees longitude and latitude. This is required since the area of a cell is dependent on latitude. To determine this area, firstly the area to the equator per latitude value is determined by including Earth's polar radius, Earth's eccentricity and the latitude values per GeoTIFF file. The distances between latitudes is then the difference of the distances to the equator. Multiplying the distances between latitudes with the distance between meridians (pixelwidth divided by 360 degrees, making it dimensionless) ultimately gives the area

per pixel in square meters. This GeoTIFF file containing the area per cell is then multiplied with the reclassified GeoTIFF file to obtain the flooded area for every flooded cell. Since flooded cells are given a value of 1 and non-flooded cells a value of 0 in the reclassified GeoTIFF, multiplication of the reclassified GeoTIFF with the GeoTIFF containing the areas per cell results in only values of zero for non-flooded cells (Figure 3.3).

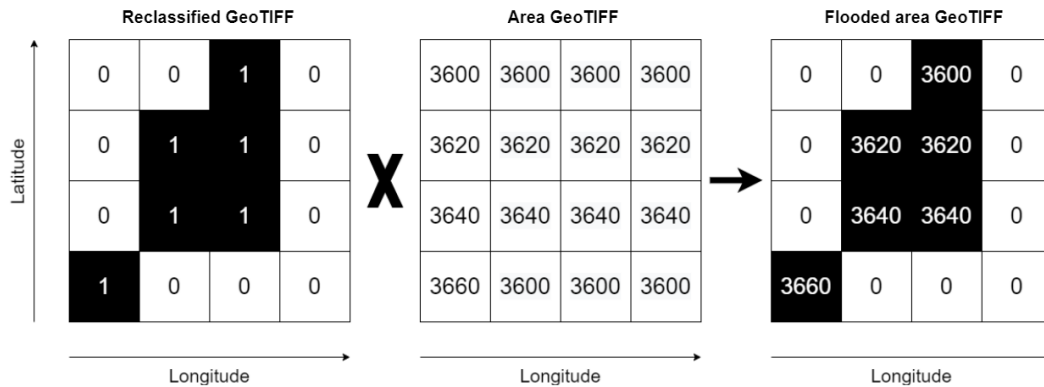


Figure 3.3: Steps to come to the flooded area on a pixel level per GeoTIFF file of 5 by 5 degrees longitude and latitude. From left to right: the reclassified GeoTIFF where a value 1 corresponds to a flooded cell; the area GeoTIFF containing the area of a cell in m²; and the flooded area GeoTIFF containing the area of a flooded cell.

3.2 Differences flooded area based on administrative boundaries

In this phase, the flooded area estimated by both models is compared based on administrative boundaries. This comparative assessment is applied on the baseline model results to identify the largest and smallest differences in estimated flood extent. All baseline return periods, corresponding to the total water levels of the return periods, will be included.

Categorizing based on administrative boundaries is applied as a first order subdivision. In this way, it can be investigated whether both models estimate a similar global pattern and magnitude of the flood hazard. Normalizing the flooded area per shoreline length is performed to increase the comparability of countries with different shoreline lengths. These shoreline lengths are gathered from the World Resources Institute (Burke et al., 2001). Furthermore, the absolute and factor difference (Bathtub/LISFLOOD-AC) in estimated flood extent (both absolute [km²] and normalized [km²/km]) between the Bathtub approach and the LISFLOOD-AC model are determined. Through this categorization, the most and least substantial differences in simulated flood hazard between the two models can be identified on a spatial basis.

To obtain the flooded area per country on a global scale, the administrative boundaries from the Database of Global Administrative Areas (GADM) is used ('GADM', n.d.). The flooded area GeoTIFF files are used as input to the GADM boundaries to determine the flood extent per country on a global scale. This is established by summing up all values in the flooded area GeoTIFF file and assigning these to the polygon of a specific country (Figure 3.4).

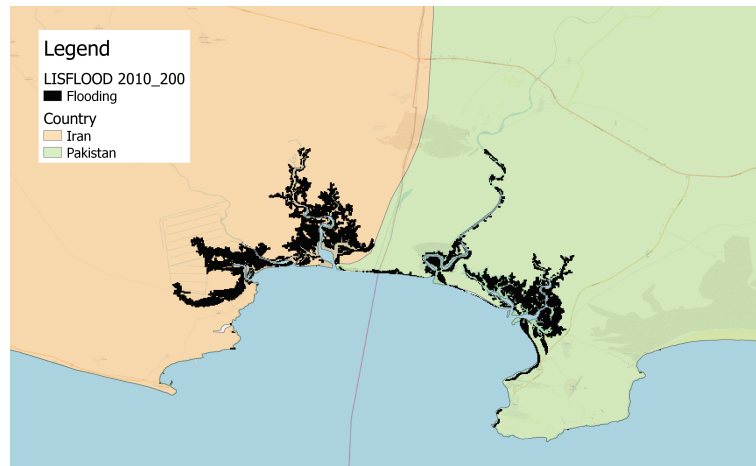


Figure 3.4: Division of the flooded area based on administrative boundaries from GADM - Example of the border between Iran and Pakistan. The flooded area is represented by the dark area on the map, the orange area represents a region of Iran and the green area represents a region of Pakistan as derived from the GADM database.

Trapezoidal numerical integration

To make comparison between countries and regions possible while including all baseline return periods, trapezoidal numerical integration is applied (Figure 3.5). This is a method to approximate the definite integral, which gives the area under the curve. The integration happens in sequence along the return periods (Eq. 3.1).

$$\int_t y(t)dt = \int_t y(t) \frac{dx}{dt} \Big|_{x=x(t)} dt \quad (3.1)$$

, with y being the FA values in this case and x the probability (1/return period) corresponding to the y (FA) values.

In this way, for each administrative area a value representing the Estimated Annual Flooded Area (EAFA) in square kilometers is determined.

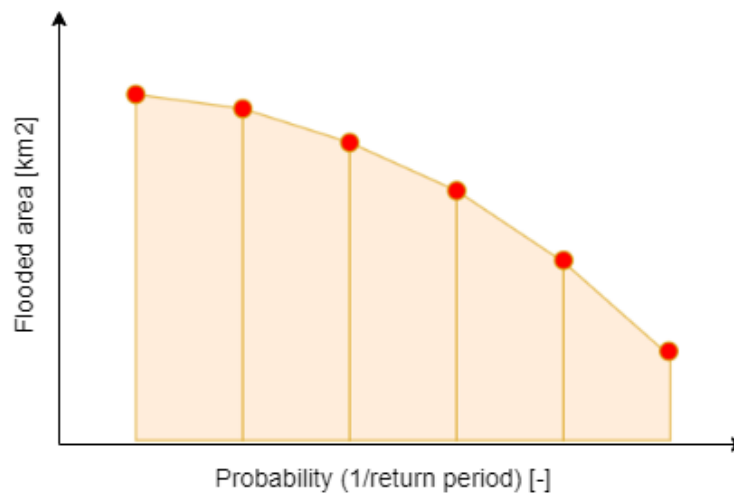


Figure 3.5: Trapezoidal numerical integration, applied to every combination of probability (1/return period) and the corresponding flooded area to determine the Expected Annual Flooded Area (EAFA).

Fit metrics

To compare the two flooding models on a country level, the metrics hit ratio, false alarm ratio and critical success index are applied. In the equations for these metrics, the LISFLOOD-AC model results are used as the 'observed' ones, assuming these results to be more accurate based on previously performed research.

The hit ratio is determined to define the cells for which the Bathtub approach estimates flooding or not, for cells where the LISFLOOD-AC model simulated flooding. Therefore, this is a metric of agreement between the two models (Alfieri et al., 2014; Bates & De Roo, 2000).

$$\text{Hit ratio} = \frac{Fm \cap Fo}{Fo} \times 100 \quad (3.2)$$

, where $Fm \cap Fo$ characterizes the flooded area correctly predicted by the Bathtub approach and Fo defines the total flooded area as estimated by the LISFLOOD-AC model.

The false alarm ratio defines whether the Bathtub approach estimates flooding in areas where the LISFLOOD-AC model does not. This is therefore a metric of disagreement (overestimation by the Bathtub approach) between the two models.

$$\text{False alarm ratio} = \frac{Fm/Fo}{Fo} \times 100 \quad (3.3)$$

, where Fm/Fo defines the area for which the Bathtub approach predicts flooding and the LISFLOOD-AC model does not.

The critical success rate is a metric defining the area correctly predicted by Bathtub as a proportion to the area for which one or both models predicts flooding (the union).

$$\text{Critical success index} = \frac{Fm \cap Fo}{Fm \cup Fo} \times 100 \quad (3.4)$$

, where $Fm \cup Fo$ (the union) characterizes the total area for which one or both models predict flooding.

These metrics are determined on a country level to determine whether the Bathtub approach estimates agree with the LISFLOOD-AC model estimates. In this, the hit rate defines if the Bathtub approach estimates flooding in the same areas as the LISFLOOD-AC model. The false alarm rate determines the degree of overestimation by the Bathtub approach, compared to the LISFLOOD-AC model. Finally, the critical success index defines the area correctly predicted by Bathtub, as a proportion to the combined flooded area of both approaches (the union).

3.3 Differences flooded area per coastal typology

Since the administrative boundaries used in the first phase of the research project are just artificial man-made boundaries, a comparison of both models based on physiographic features is performed to argue the usefulness of the two methods. Therefore, differences in estimated flood extent for varying types of areas are distinguished. In this way, any influence of the physical nature of the coastline on the accuracy of the models is investigated. All baseline return periods are included again. Furthermore, the flooded area GeoTIFF files are used again in this phase. To make comparison between the different coastline types possible, the factor difference (Bathtub/LISFLOOD-AC) is determined as well as the percentage of contribution to the total global difference. Furthermore, the fit metrics (Hit rate, false alarm rate and critical success index) are determined based on the coastal typology classes.

A global dataset with information of the physical state of the coastline is required to allocate the flooded area to a certain shoreline type. An overview by Dürr et al. (2011) containing nine different coastal types is used. These coastal types are classified based on hydrological, lithological and morphological criteria. The nine different coastal types are presented in Table 3.1. A brief description of the coastal typologies and the steps performed to classify them is presented in Appendix A.1. The classes will be referred to by their name without the number of the typology.

Table 3.1: Coastal typology classes from Dürr et al. (2011). With FIN_TYP as an ID of the coastal typology; coastal typology representing the name of the coastal type; the coastline length per coastal typology in [km]; and the percentage of the coastal typology to the global coastline length in [%]. *The coastal typologies Large Rivers and Large rivers with tidal deltas together cover 0.7% of the global coastline length.

FIN_TYP	Coastal typology	Coastline length [km]	Percentage of global coastline [%]
0	Endorheic or Glaciated	24469	5.6
1	Type I Small deltas	131167	30.1
2	Type II Tidal systems	91326	21
3	Type III Lagoons	33286	7.6
4	Type IV Fjords and fjaerds	105657	24.3
5	Non-filter Type Va Large Rivers	1491.949	0.7*
6	Non-filter Type VI Karst	10543	2.4
7	Non-filter Type VII Arheic	35979	8.3
51	Non-filter Type Vb Large Rivers with tidal deltas	1389.056	0.7*

The global distribution of the coastal typology is displayed in Figure 3.6.

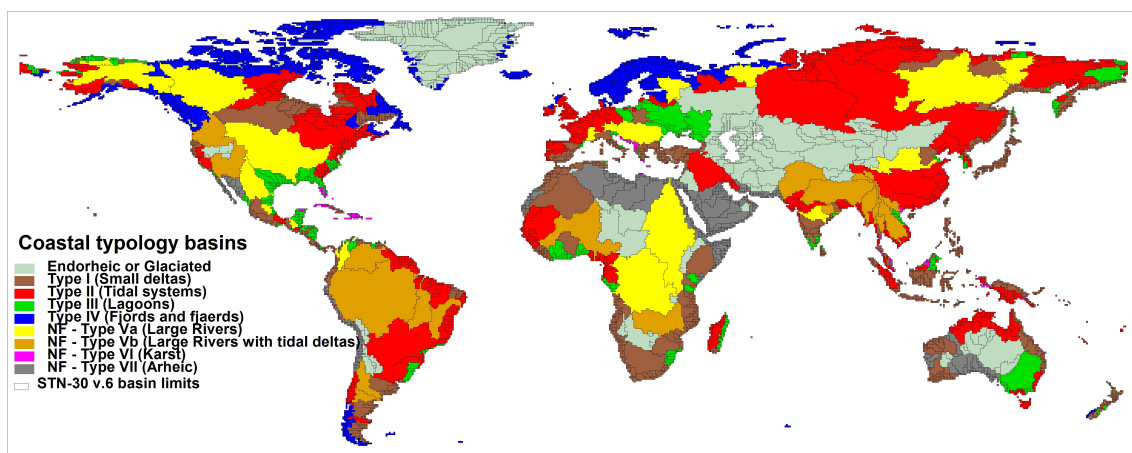


Figure 3.6: Global distribution of the coastal typology basins, from Dürr et al. (2011).

3.3.1 Coastal typology database pre-processing

The coastal typology data is available in a resolution of 0.5 degrees longitude and latitude. This makes that the coastline shows a rough pattern which would result in neglecting parts of the flooding data when using this shapefile to determine the flooded area. Therefore, the coastal typology data is combined with the GADM boundary layer. However, due to the difference in resolution this results in numerous small areas to which no coastal typology class is assigned. Keeping these areas without a coastline classification would result in a total of 25% of the global flooded area being assigned to an area with no coastal typology class. To be able to include this 25% in the investigation of the flooded area per typology class, nearest neighbor interpolation is applied (Figure 3.7).



Figure 3.7: Applying nearest neighbor interpolation to assign coastal typology classes to areas which have none after combining the coastal typology data with the GADM data. Left picture shows the combined layer before and right picture shows the layer after nearest neighbor interpolation was applied.

The shapefile containing the global coastal typologies is cut in 5-by-5 degree files to overlay them with the flooding results. The flooded area is then computed the same way as the computation of the flooded area on a country level.

3.4 Differences flooded area per terrain class

Since the terrain of the flood prone area influences the flood propagation, a comparative analysis between the Bathtub approach and the LISFLOOD-AC model for different terrain classes is applied. Again, the differences in estimated flood extent between the two models are investigated on a global scale. A global dataset covering 15 terrain classes, available in a resolution of 280 meters, is used in this analysis (Iwahashi et al., 2018). A brief description of the terrain classes and the steps performed to classify them is presented in Appendix A.2. The presence of the terrain classes is shown in Figure 3.8.

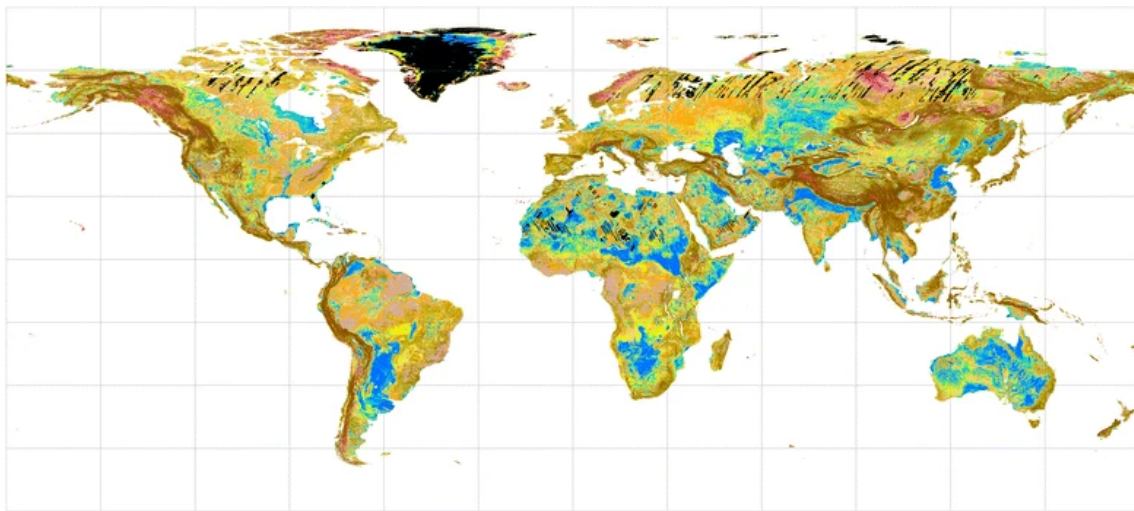


Figure 3.8: Global overview of terrain classification from Iwahashi et al. (2018). Colours in Table 3.2 represent the legend for the figure.

The terrain classification data was created with the use of the multi-error-removed improved-terrain DEM (MERIT DEM), resulting in a polygon-based dataset. The errors removed include absolute bias, stripe noise, speckle noise and tree height bias which were corrected with the use of multiple satellite datasets and filtering techniques (Yamazaki et al., 2017). The three main classification variables included to establish the terrain classes are the slope gradient, the local convexity and surface texture. Area segmentation was applied, using the logarithmic value of slope gradient and the local convexity. Next, surface texture was included by k-means clustering and the resulting polygons were grouped into 40 clusters. These 40 clusters were compared with Japanese geological

and geomorphological data to reclassify them into 12 groups with different characteristics. Three subgroups were added for large shape landforms, mountains and hills based on the combined texture. This makes a total of 15 terrain groups, present in Table 3.2.

Table 3.2: Global terrain classes from Iwahashi et al. (2018). Colours represent the legend for Figure 3.8. The 15 terrain classes are represented by an ID in the Terrain group column and a definition in the Landform pattern column. The classes are subdivisions of the five overview groups presented in the column Overview. In Typical landforms in Japan some landforms corresponding to the landform pattern classes are presented which are typically observed in Japan.

Overview	Terrain group	Landform pattern	Typical landforms in Japan
Bedrock mountain	1a	Steep mountain (rough)	steep mountain of accretionary complex / un-decomposed plutonic rock
	1b	Steep mountain (smooth)	steep mountain of felsic / dissected mafic volcano, escarpment of caldera / fault-block mountain, inselberg
	2a	Moderate mountain (rough)	moderate mountain of felsic volcanic rock / accretionary complex
	2b	Moderate mountain (smooth)	moderate mountain of old sedimentary rock / dissected mafic volcano
Hills	3a	Hills (rough in small and large scale)	hills and mountain footslope of weathered rock
	3b	Hills (smooth in small scale, rough in large scale)	hills of pyroclastic flow deposits / Tertiary sedimentary rock, talus
Large highland slope	4	Upper large slope	un-dissected mafic volcano
	5	Middle large slope	volcanic footslope of debris, dissected escarpment of sediments
Plateau, terrace, large lowland slope	6	Dissected terrace, moderate plateau	hilly terrace, metropolitan areas and coastal industrial areas
	7	Slope in and around terrace or plateau	terrace edge or valley bottom plain in and around terrace
	8	Terrace, smooth plateau	terrace, sand bar, metropolitan areas and coastal industrial areas
	9	Alluvial fan, pediment, bajada, pediplain	alluvial fan, dissected alluvial fan
Plain	10	Alluvial plain, pediplain	alluvial plain in upstream
	11	Alluvial or coastal plain, pediplain	alluvial plain, coastal lowland
	12	Alluvial or coastal plain (gentlest), lake plain, playa	delta, marsh, coastal lowland

Again, differences in estimated flooded area by both models are determined. These are established as differences in square kilometers (Bathtub - LISFLOOD-AC), factor differences (Bathtub/LISFLOOD-AC) and the percentage of contribution to the total global difference. Furthermore, the fit metrics (Hit rate, false alarm rate and critical success index) are determined based on the terrain classes.

3.4.1 Terrain classes database pre-processing

The database by Iwahashi et al. (2018) is clipped in 5-by-5-degree GeoTIFF files, matching the extent of the flooding results. This ensures that the flooded area per terrain class can be determined iterative over all model outcome GeoTIFF files. The terrain classification dataset is available in a 280 m resolution. Therefore, the terrain classes database is translated into the same resolution as the flooding data (8.3×10^{-4} degrees) using GDAL translate. For the calculation of the flooded area per terrain class, the GeoTIFFS covering the terrain classes are transformed to shapefiles using the GDAL polygonize tool, which is a command line tool to produce a polygon feature layer from a raster. Next, these shapefiles are merged with the GADM boundaries to ensure that the same shoreline position is taken into account as used in the comparison based on administrative boundaries and coastal typologies. This merge is established by executing an intersection, which is a type of vector overlay that results in a layer combining the features of both input layers for all intersecting areas.

4 | Results

In this chapter the results of the global comparative study of the flood extent estimates by the Bathtub approach and the LISFLOOD-AC model are presented, arising from the methodology presented in Chapter 3. This starts with an overview of the flooded area on a country level both in terms of flooded area [km²] and flooded area normalized by shoreline length [km²/km]. Subsequently, the differences between the two modelling approaches are discussed. The second part of this chapter presents the estimated flood extent per coastal typology class. The chapter ends with an overview of the results based on terrain classes.

4.1 Flood extent based on administrative boundaries

4.1.1 Flooded area per country

Based on the administrative boundaries from the GADM database ('GADM', n.d.), the flooded area (FA) per country is established. This FA is determined for all six baseline return periods summarised in Table 2.1 and for both the Bathtub approach as the LISFLOOD-AC model flooding results.

The FA per country for all Bathtub approach baseline return periods is presented in Figure 4.1. The global pattern observed stays relatively uniform, with gradual increases when moving from lower to higher return periods of ESLs. However, sudden, catastrophic flooding at higher return periods of ESLs is seen in e.g. the United States. Based on FEMA guidelines for insurance ('Special Flood Hazard Area (SFHA) | FEMA.gov', n.d.), a primary flood protection standard of a 100-year return period is implemented all around the USA in the models, which causes this sudden increase in estimated flooded area for an ESL with a return period of 200 years.

However, sudden, catastrophic flooding at higher return periods of ESLs is seen in e.g. the USA. Based on FEMA guidelines for insurance, a primary flood protection standard of a 100-year return period is implemented all around the USA, which causes this sudden increase in estimated flooded area for an ESL with a return period of 200 years.

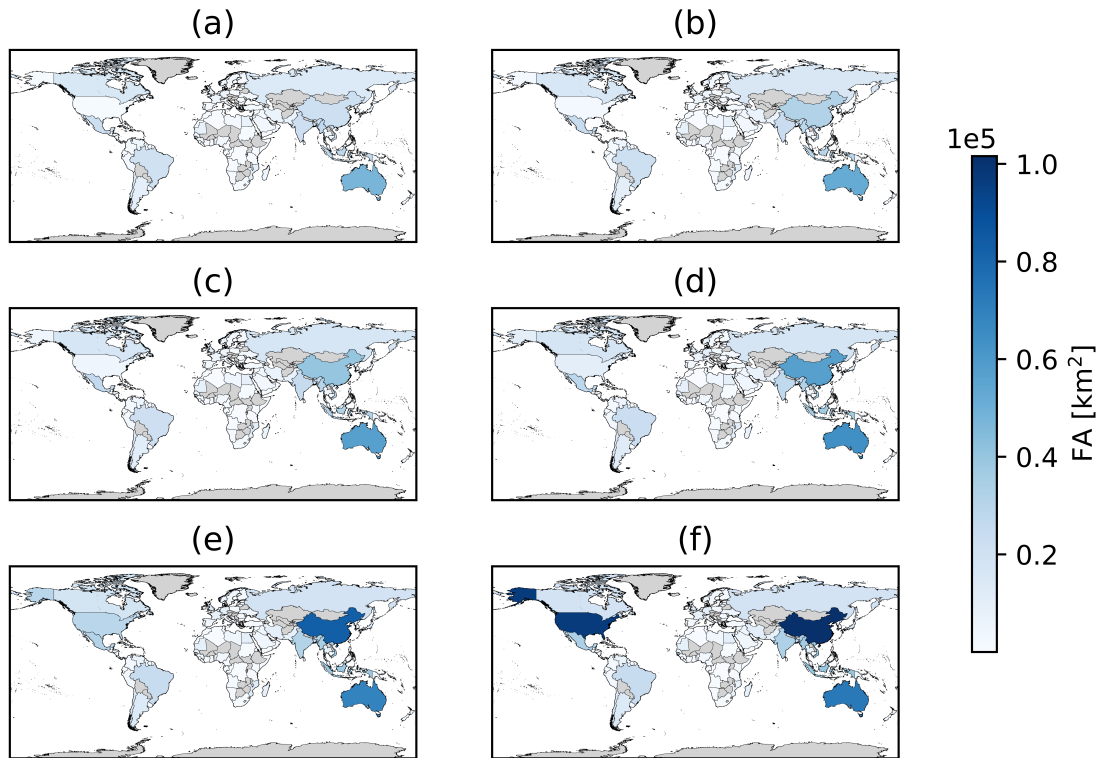


Figure 4.1: FA per country for all Bathtub approach baseline return periods. With (a) the estimates for the 5-year event; (b) the 10-year event; (c) the 20-year event; (d) the 50-year event; (e) the 100-year event; and (f) the 200-year event.

Applying numerical trapezoidal integration (Section 3.2) to the FA values spanning the 5-200 year baseline return periods provides the Estimated Annual Flooded Area (EAFA). These EAFA values for the Bathtub approach are presented in Figure 4.2.

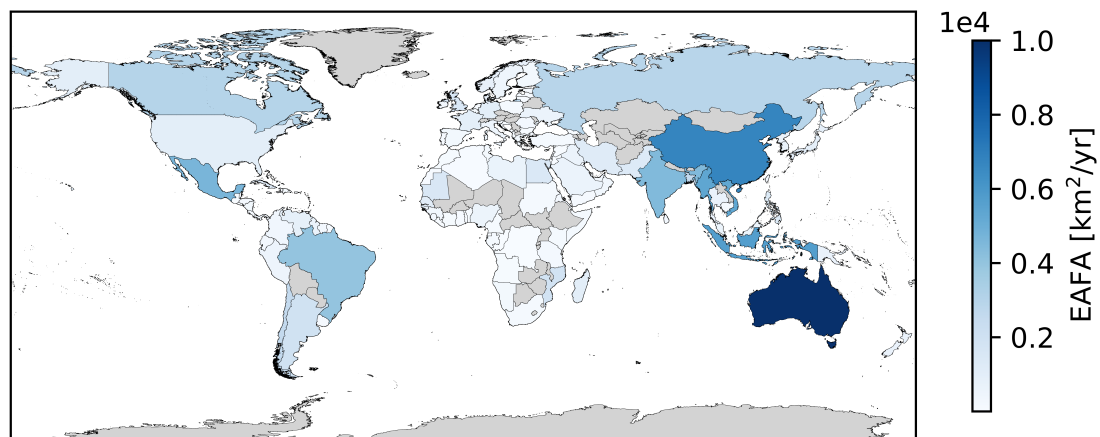


Figure 4.2: EAFA per country spanning all Bathtub approach baseline return periods.

From this map it can be observed that the highest EAFA values are estimated for countries in Asia and Australia. The top five countries with the highest EAFA estimated by the Bathtub approach for the baseline events are presented in Table 4.1. Four of these five countries are located in Asia.

Table 4.1: Top five countries with the largest EAFA for the baseline return periods as estimated by the Bathtub approach.

Country name	EAFA [km^2/yr]
Australia	10550
China	7093
Indonesia	6056
Myanmar	5673
Vietnam	5623

The FA estimates spanning the 5-200 year baseline return periods as estimated by the LISFLOOD-AC model are presented in Figure 4.3. From these maps, a similar spatial pattern, with Fa increasing as ESL increases, can be observed as was established from the Bathtub approach results. However, the magnitude of estimated FA is generally lower by the LISFLOOD-AC model than that computed by the Bathtub approach for the same return period. Especially for lower return periods of ESLs, the estimated flooding by the LISFLOOD-AC model remains low compared to the Bathtub approach projections. This can be explained by the difference in the forcing ESL in both modelling approaches. The lower return period ESLs from the triangular synthetic hydrograph used in the LISFLOOD-AC computation will only exceed the land elevation for a short period of time while in the Bathtub approach this temporal component is not included. This results in a different magnitude of potential flood waters, since the available flood volume in the Bathtub approach is larger than for the LISFLOOD-AC model. The sudden increases in estimated flooded area when moving to higher return periods of ESLs are observed again for some countries (e.g. USA), as a result of the effect of the inclusion of flood protection in the models.

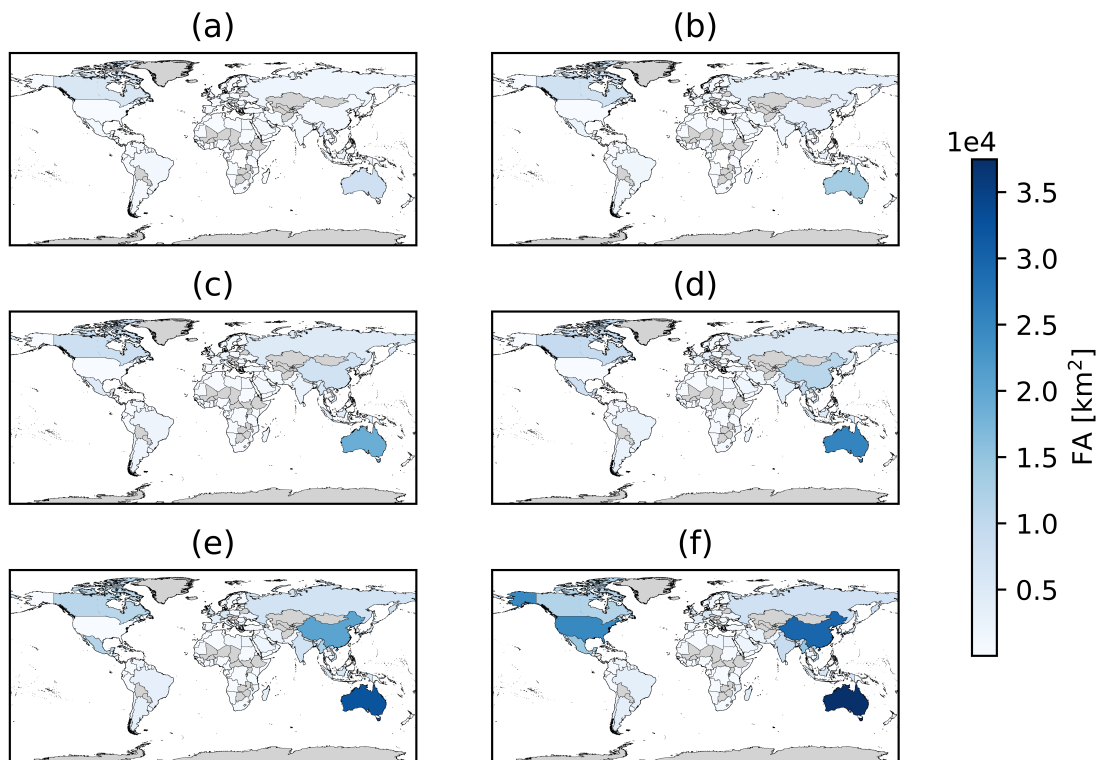


Figure 4.3: FA per country for all baseline return periods as estimated by the LISFLOOD-AC model. With (a) the estimates for the 5-year event; (b) the 10-year event; (c) the 20-year event; (d) the 50-year event; (e) the 100-year event; and (f) the 200-year event.

The EAFA values as estimated by the LISFLOOD-AC model are shown in Figure 4.4.

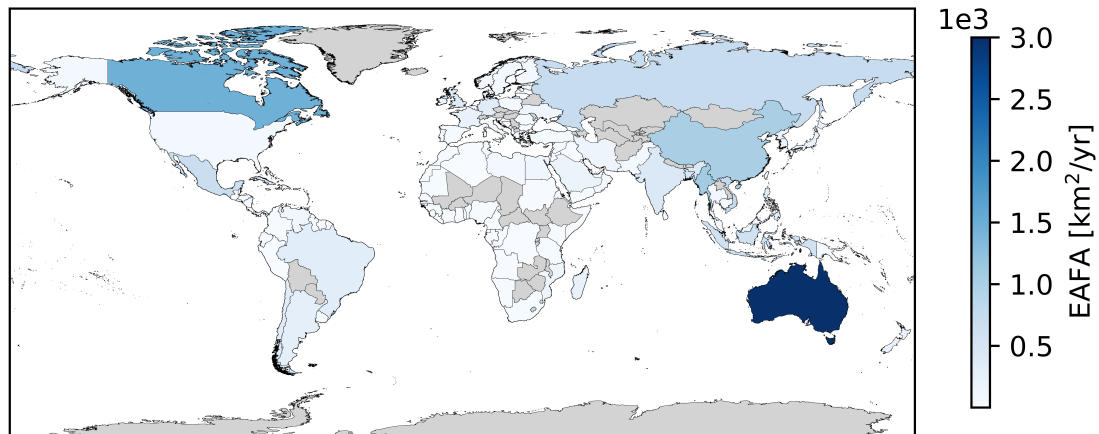


Figure 4.4: EFAFA per country spanning all LISFLOOD-AC baseline return periods.

From this EFAFA map for LISFLOOD-AC, it is observed that the global pattern is relatively similar to that estimated by the Bathtub approach, although Canada now stands out more. When looking at the top five countries with the highest estimated EFAFA values (Table 4.2), it is clear that, with the exception of Canada, all of the countries in the top five are the same as those estimated by the Bathtub approach.

Table 4.2: Top five countries with the largest EFAFA spanning all baseline return periods as estimated by the LISFLOOD-AC model.

Country name	EFAFA [km ² /yr]
Australia	3001
Canada	1468
Myanmar	1081
China	1012
Vietnam	766

4.1.2 Flooded area per country, normalized by shoreline length

The FA per country is normalized by shoreline lengths gathered from the WRI (Burke et al., 2001). The normalized EFAFA values based on all the Bathtub approach baseline return periods are shown in Figure 4.5. The global pattern is very different to that shown in Figures 4.1 and 4.2.

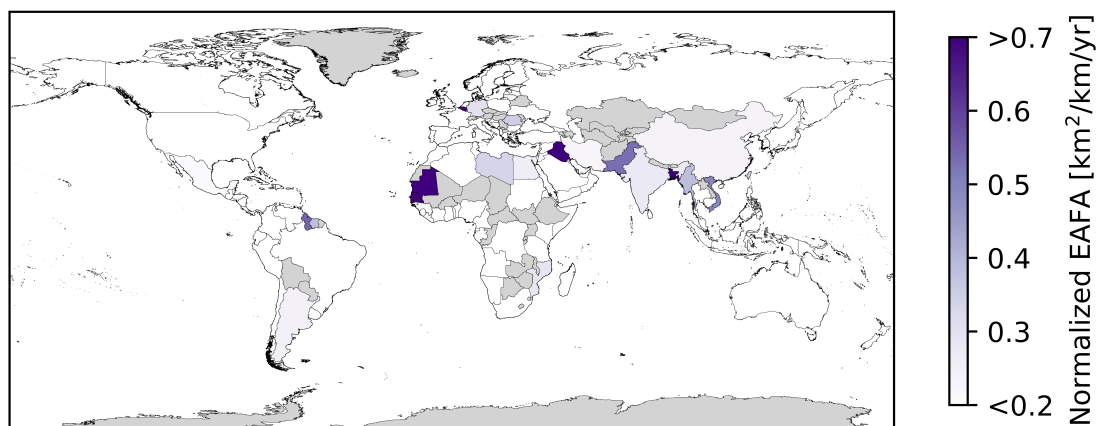


Figure 4.5: Normalized EFAFA spanning all the Bathtub approach baseline return periods.

One country that has an exceptionally high normalized EAFA is Iraq. With a shoreline length of 105 km and an EAFA of 640.6 km²/yr based on all baseline return periods, a normalized EAFA of 6.10 km²/km/yr is estimated by the Bathtub approach. The top five countries with the highest estimated normalized EAFA for the Bathtub approach baseline return periods are presented in Table 4.3.

Table 4.3: Top five countries with the largest normalized EAFA spanning all baseline return periods as estimated by the Bathtub approach.

Country name	Normalized EAFA [km ² /km/yr]
Iraq	6.10
Mauritania	1.28
Senegal	0.85
Bangladesh	0.83
Guyana	0.55

Normalizing the EAFA for all countries by their corresponding shoreline length results in Figure 4.6.

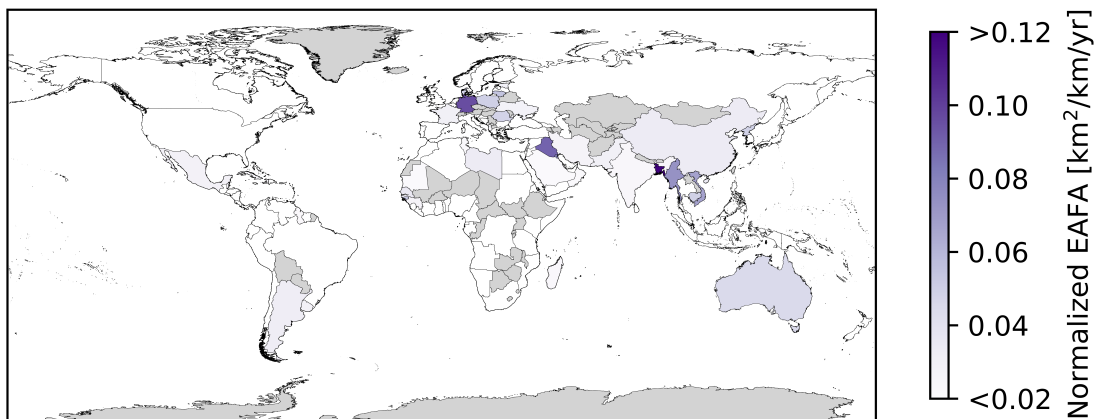


Figure 4.6: Normalized EAFA spanning all LISFLOOD-AC baseline return periods.

The country showing the highest value of normalized EAFA as estimated by the LISFLOOD-AC model spanning all baseline return periods is Bangladesh, with a value of 0.14 km²/km/yr. The top five countries for these normalized EAFA values are shown in Table 4.4. This top five has two countries in common with the top five as estimated by the Bathtub approach: Iraq and Bangladesh.

Table 4.4: Top five countries with the largest normalized EAFA spanning all baseline return periods as estimated by the LISFLOOD-AC model.

Country name	Normalized EAFA [km ² /km/yr]
Bangladesh	0.14
Germany	0.10
Iraq	0.09
Kuwait	0.08
Myanmar	0.07

4.1.3 Differences in flood extent

When comparing the global flood maps of the Bathtub approach with those from the LISFLOOD-AC model, the global pattern in estimated flooded area is relatively similar while the magnitude differs significantly (Figure 4.7). This implies that the topography, which is the only variable included in the Bathtub approach, determines whether an area will be flooded or not. However, other variables like surface roughness are crucial to estimate the magnitude of the flood extent.

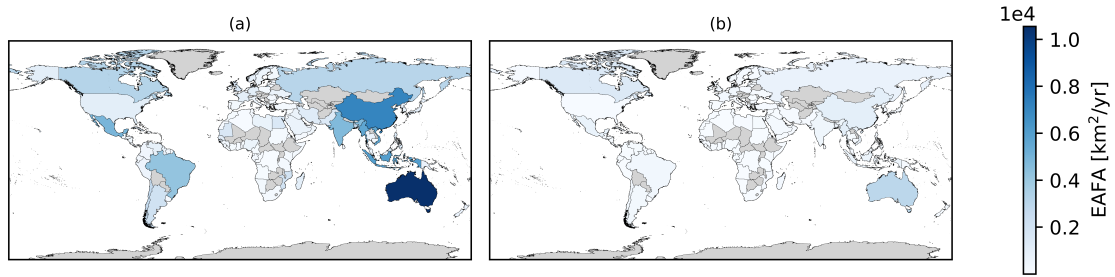


Figure 4.7: EFAA estimates from (a) the Bathtub approach and (b) the LISFLOOD-AC model, spanning all baseline return periods. Both EFAA maps are shown using the same colorbar.

In Table 4.5 the top five countries with the largest positive difference (overestimation by the Bathtub approach) in normalized flooded area on a country level are presented for the baseline 100-year event. This shows that the largest differences in EFAA are observed for countries in Asia and Oceania. Furthermore, Northern Cyprus is the only country for which the LISFLOOD-AC model estimates a higher EFAA. However, with a difference of just $0.56 \text{ km}^2/\text{yr}$ this is negligible in a study on a global scale. For all other countries, the Bathtub approach overestimates the flooded area.

Table 4.5: Top five countries with the largest positive difference in EFAA spanning all baseline return periods. Computed as EFAA Bathtub - EFAA LISFLOOD-AC.

Country name	Difference EFAA [km^2/yr]
Australia	7549
China	6081
Indonesia	5450
Vietnam	4857
Myanmar	4592

When comparing both models by their normalized EFAA estimates (Table 4.6), it is observed that the top five countries with the largest differences (Bathtub - LISFLOOD-AC) changed completely. The top five is now more spread around the world and less concentrated in Asia and Oceania.

Table 4.6: Top five countries with the largest positive difference in normalized EFAA for the baseline return periods. Computed as normalized EFAA Bathtub - normalized EFAA LISFLOOD-AC.

Country name	Difference normalized EFAA [$\text{km}^2/\text{km}/\text{yr}$]
Iraq	6.01
Mauritania	1.26
Senegal	0.81
Bangladesh	0.69
Guyana	0.52

Mapping the factor difference between the Bathtub approach and the LISFLOOD-AC model estimates of the EFAA per country shows us that the Bathtub approach generally overestimates (Figure 4.8). The factor difference in these maps is calculated as $(\text{EFAA Bathtub}/\text{EFAA LISFLOOD-AC})$. Although the Bathtub approach overestimates the flood extent compared to the LISFLOOD-AC model, the degree of overestimation varies substantially among countries, with a minimum factor difference in EFAA of 1.1 for Syria and a maximum factor difference of 253 for São Tomé and Príncipe.

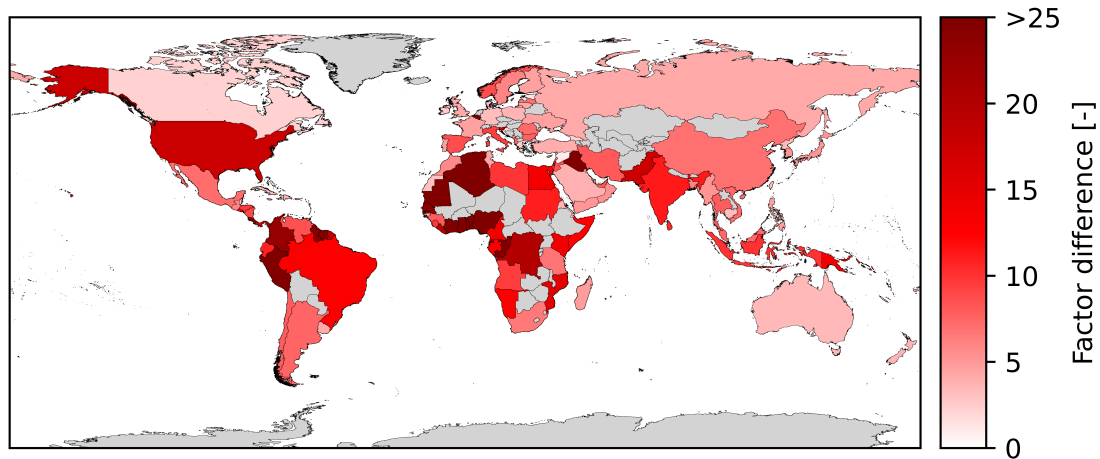


Figure 4.8: Factor difference in estimated EAFA between the Bathtub approach and the LISFLOOD-AC model for all baseline return periods. This difference is computed as $\text{EAFA}_{\text{Bathtub}} / \text{EAFA}_{\text{LISFLOOD-AC}}$.

To investigate the spread in the factor difference in estimated EAFA between both models, a box plot is created (Figure 4.9).

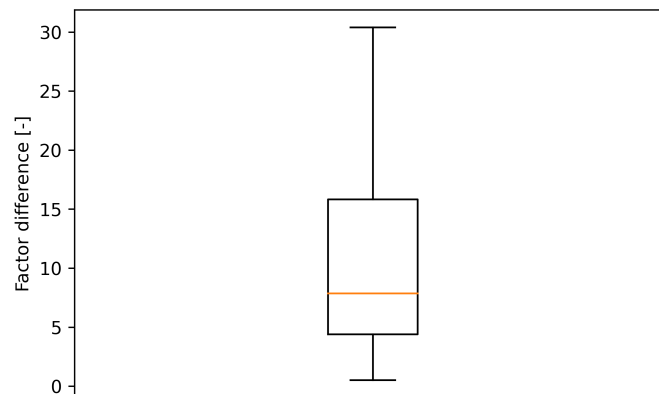


Figure 4.9: Boxplot of factor difference in EAFA per country between the Bathtub approach and the LISFLOOD-AC model for all baseline return periods. The orange line represents the median factor difference, the box the interquartile range (IQR, 25th (Q1) to 75th (Q3) percentile) and the outer lines represent the minimum ($Q1 - 1.5 \cdot \text{IQR}$) and maximum values ($Q3 + 1.5 \cdot \text{IQR}$).

This box plots illustrates the spread in factor difference in EAFA per country, with a median value equal to 7.9 and the interquartile range (IQR), representing the 25th to 75th percentile, spanning from 4.4 to 15.8. This implies that a large spread is observed for the factor difference in EAFA per country, as estimated by the Bathtub approach and the LISFLOOD-AC model. The lower bound of the IQR represents an overestimation by the Bathtub approach of 4.4 times the EAFA as estimated by the LISFLOOD-AC model, implying large overestimation by the Bathtub approach for most of the countries.

4.1.4 Global totals

Summing the FA estimates for all countries results in the global total flooded area estimate by both modelling approaches. For each return period, this global FA estimate by the Bathtub approach and the LISFLOOD-AC model is presented in the bar plots in Figure 4.10. It can be observed that the magnitude in FA increases when the return period of the ESL increases, although the increase rate differs between both models. The total global difference in FA between the baseline 200-year

event and the 5-year event is 84.7% for the Bathtub approach and 524.5% for the LISFLOOD-AC model.

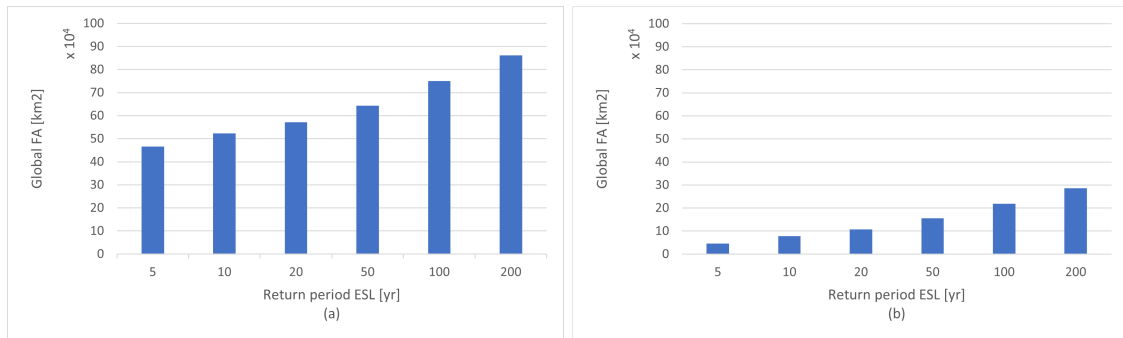


Figure 4.10: Global total FA as estimated by the Bathtub approach (a) and the LISFLOOD-AC model (b) spanning all baseline return periods.

When determining the total global difference in FA per return period between the Bathtub approach and the LISFLOOD-AC model, this shows that the increase in difference in FA shows a linear relation with the return period of the ESLs. Displaying the factor difference per ESL results in bar plots with a decreasing value when moving to higher return periods of ESLs. This implies that the factor difference between both models decreases for extreme events with a higher return period. Reason for this could be the effect of flooding in coastal plains, since even for lower return period ESLs the flooded area estimated by the Bathtub approach is large since only the topography is taken into account. When moving to higher return periods of ESLs the area might not increase significantly while the flood volume does.

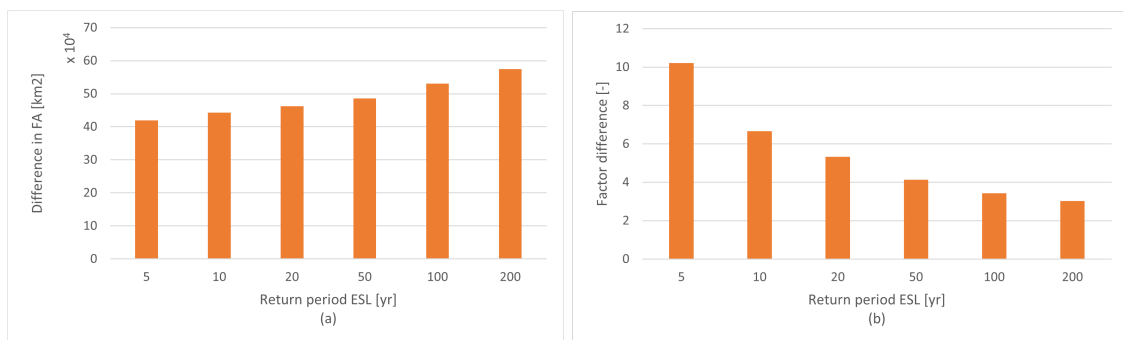


Figure 4.11: (a) Difference in global total FA (Bathtub - LISFLOOD-AC) and (b) factor difference in FA (Bathtub/LISFLOOD-AC) values per baseline return period.

4.1.5 Fit metrics

The results of the fit metrics on a country level are presented in this section. This includes the hit ratio, false alarm ratio and critical success index. The values were computed on a country level for each baseline return period, according to the formulas presented in Section 3.

The minimum and maximum hit rate per country over all baseline return periods is presented in Figure 4.12. The hit rates are calculated using Eq. 3.2. These maps illustrate that for most countries included in the analysis the hit rate is significantly high: 80% of the countries has a minimum value of at least 75% and a maximum value of at least 90%. This implies that the Bathtub approach generally estimates flooding in areas for which the LISFLOOD-AC model does as well.

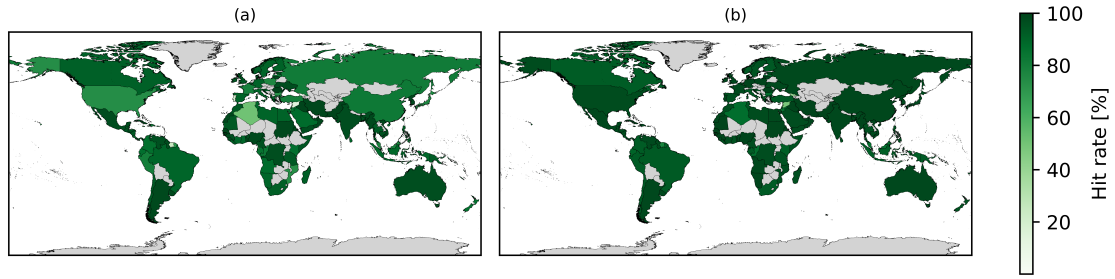


Figure 4.12: Minimum (a) and maximum (b) values for the hit rate per country over all baseline return periods.

The maps displaying the minimum and maximum false alarm rates per country over all baseline return periods can be seen in Figure 4.13. The false alarm rates are calculated using Eq. 3.3. A total of 30 countries has a minimum value higher than 1000%. For the maximum values of the false alarm rate, this includes 105 countries. These large values for the false alarm rate correspond to large overestimation in estimated flooded area by the Bathtub approach, when comparing the estimates with the LISFLOOD-AC model results.

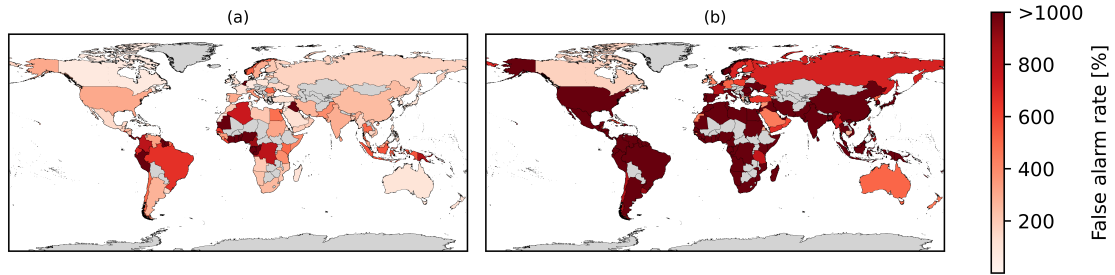


Figure 4.13: Minimum (a) and maximum (b) values for the false alarm rate per country over all baseline return periods.

Minimum and maximum values per country for the critical success index over all baseline return periods are displayed in Figure 4.14. The critical success index values are calculated using Eq. 3.4. The values for the critical success index are substantially lower than those established for the hit rate: only two countries have a minimum value for the critical success index higher than 50%. For the maximum critical success index values this includes 23 countries. The low values for the critical success index represent a low degree of agreement between the flooded area estimates of the Bathtub approach and the LISFLOOD-AC model.

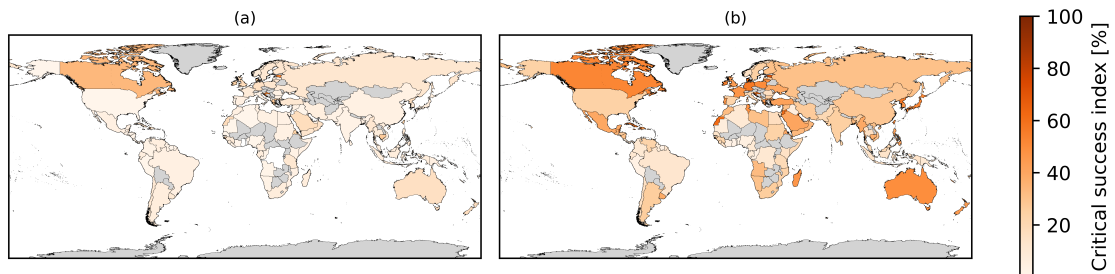


Figure 4.14: Minimum (a) and maximum (b) values for the critical success index per country over all baseline return periods.

4.2 Flood extent per coastal typology

In this section, the flooded area per coastal typology is determined. Based on nine different classes, a distinction is made between coastlines. The results are again established for all baseline return periods, for both the Bathtub approach and the LISFLOOD-AC model.

4.2.1 Flooded area per coastal typology

The EAFA values per coastal typology are presented for both the Bathtub approach as the LISFLOOD-AC model in Table 4.7.

Table 4.7: EAFA values per coastal typology as estimated by the Bathtub approach and the LISFLOOD-AC model.

Coastal typology	Bathtub EAFA [km ² /yr]	LISFLOOD-AC EAFA [km ² /yr]
0. Endorheic or Glaciated	460	35
1. Type I Small deltas	21625	3025
2. Type II Tidal systems	45363	5923
3. Type III Lagoons	10184	1126
4. Type IV Fjords and fjaerds	6513	997
5. Non-filter Type Va Large Rivers	1511	43
6. Non-filter Type VI Karst	2929	477
7. Non-filter Type VII Arheic	7925	900
51. Non-filter Type Vb Large Rivers with tidal deltas	4538	178

To visualize the EAFA values, a bar plot is created (Figure 4.15). From this figure it is observed that the largest EAFA values are estimated for the same coastal typologies by both models, although the magnitude differs significantly.

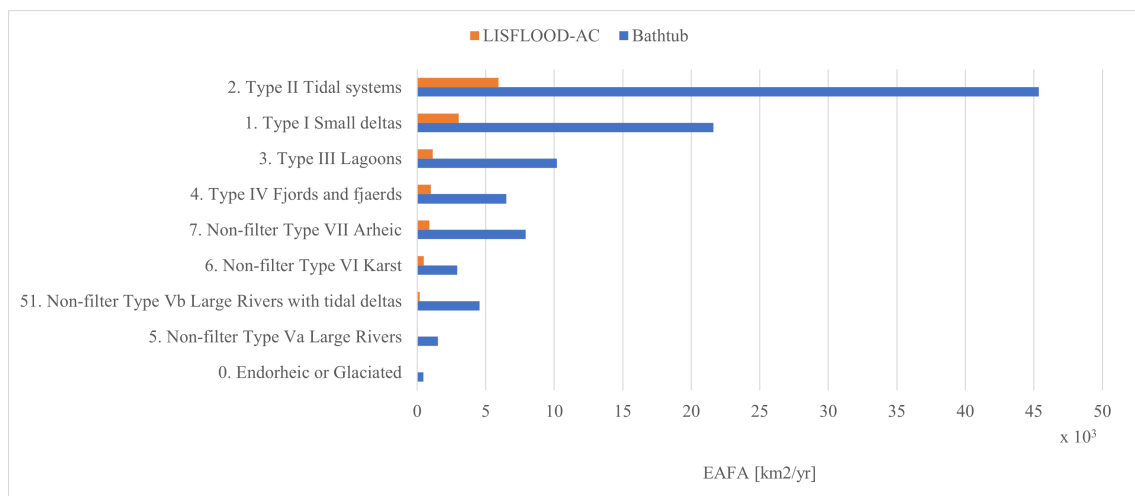


Figure 4.15: Total Estimated Annual Flooded Area (EAFA) per coastal typology class as estimated by the Bathtub approach and the LISFLOOD-AC model.

The coastal typology classes are not equally distributed along the global coastline. Therefore, the EAFA values per typology are compared as factor differences. These are computed as the EAFA as estimated by the Bathtub approach divided by the EAFA as estimated by the LISFLOOD-AC model. Therefore, a positive value corresponds to overestimation by the Bathtub approach compared to the LISFLOOD-AC model. This results in the bar plot presented in Figure 4.16

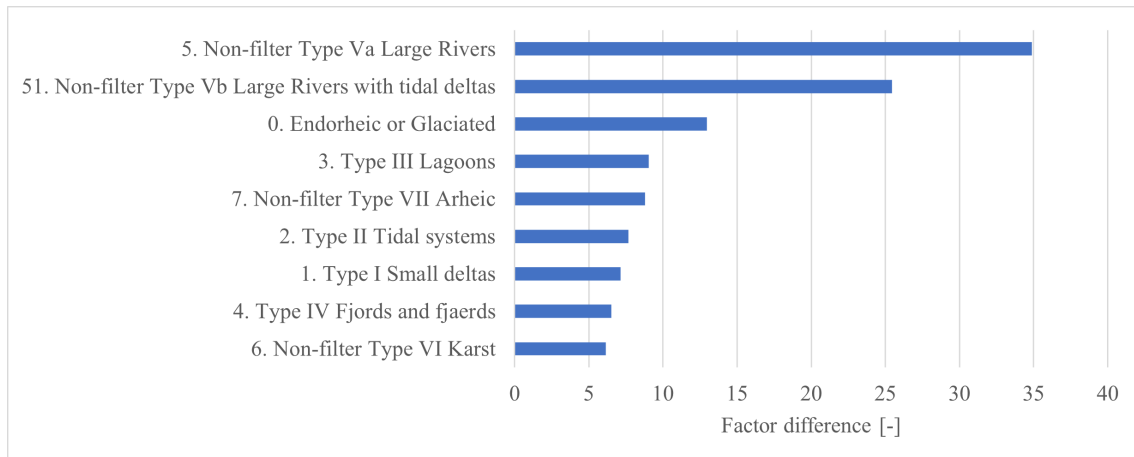


Figure 4.16: Factor difference in total EAFA per coastal typology class as estimated by the Bathtub approach and the LISFLOOD-AC model. This factor difference is computed as (EAFA Bathtub/EAFA LISFLOOD-AC).

The factor difference in EAFA as estimated by the Bathtub approach and the LISFLOOD-AC model is the largest for the typology class Large Rivers, followed by the class Large Rivers with Tidal Deltas. The corresponding values of 34.9 and 25.5 respectively, clearly represent a substantial difference in the estimated flooded area. The factor difference in EAFA is the smallest for Karst coasts, followed Fjords and fjaerds, with corresponding values of 6.1 and 6.5 respectively. This implies that the Bathtub estimates are at least 6.1 times the LISFLOOD-AC estimates in EAFA based on the different coastal typologies. The smaller factor differences observed for Karst coasts, and Fjords and fjaerds can be explained by the steeper coastline slopes of these typologies compared to the others. The influence of the topography is therefore larger which results in less overestimation by the Bathtub approach. However, since the factor difference has a minimum value of 6.1, this suggests that the Bathtub approach never provides a sufficient estimate of the flooded area based on these coastal typologies.

The absolute difference and the percentage of this difference to the total global difference in EAFA as estimated by the Bathtub approach and the LISFLOOD-AC model are determined. The absolute difference is computed as the EAFA as estimated by the Bathtub approach minus the EAFA as estimated by the LISFLOOD-AC model, implying that a positive value represents overestimation by the Bathtub approach. The proportion of this difference to the total worldwide difference indicates how much of the difference in predicted flooded area arises from a certain coastal typology. All these are presented in Table 4.8.

Table 4.8: Differences in EAFA (Bathtub - LISFLOOD-AC), factor difference in EAFA (Bathtub/LISFLOOD-AC), percentage of total difference in EAFA values per coastal typology and percentage of coastal typology to the entire global coastline length.

Coastal typology	Diff. (Bath - LIS) [km ² /yr]	Fact. Diff. (Bath/LIS) [-]	Diff. to total [%]	% of coastline
0. Endorheic or Glaciated	424	13.0	0.5	5.6
1. Type I Small deltas	18600	7.1	21.1	30.1
2. Type II Tidal systems	39439	7.7	44.6	21
3. Type III Lagoons	9058	9.0	10.3	7.6
4. Type IV Fjords and fjaerds	5516	6.5	6.2	24.3
5. Non-filter Type Va Large Rivers	1468	34.9	1.7	0.7*
6. Non-filter Type VI Karst	2452	6.1	2.8	2.4
7. Non-filter Type VII Arheic	7025	8.8	8.0	8.3
51. Non-filter Type Vb Large Rivers with tidal deltas	4360	25.5	4.9	0.7*

While the factor difference between both models is the largest for Large Rivers and Large Rivers with Tidal Deltas, this difference only includes 6.6% of the total global difference in EAFA between both models. This can be explained by the low percentage of this class to the global coastline length, since Large Rivers (both tidally influenced or not) together cover 0.7% of the global coastline length. The largest contribution to the difference in EAFA comes from Tidal systems with a corresponding

value of 44.6%.

4.2.2 Fit metrics

In Table 4.9 an overview of the fit metrics for the different coastal typology classes is outlined. The minimum; mean; and maximum value across all baseline return periods are presented. The fit metrics show high values for all of the typology classes involved, with a minimum mean value of 90.4%. This implies that for any coastal typology, the Bathtub approach estimates flooding in areas where LISFLOOD-AC estimates flooding as well. The values for the false alarm rate, representing overestimation by the Bathtub approach, are significantly high. This implies that for every coastal typology, the Bathtub approach overestimates the flooded area to a substantial degree compared to LISFLOOD-AC. The observed false alarm rates are the lowest for the Fjords and fjaerds and Karst coasts. Since these coastal typologies are characterized by steeper coastline slopes, the topography has a significant impact on the estimated flooding. This results in less overestimation by the Bathtub approach compared to the LISFLOOD-AC model estimates and therefore smaller false alarm rates are established. The critical success index shows relatively low values for all classes. Implying that there is never a sufficient agreement in flooded area estimates by both modelling approaches for any type of coastline.

Table 4.9: Fit metrics for coastal typology classes. For the metrics Hit rate, False alarm rate and Critical success index the minimum, mean and maximum value are presented, based on all baseline return periods.

Coastal typology	Hit rate [%]			False alarm rate [%]			Critical success index [%]		
	<i>Min</i>	<i>Mean</i>	<i>Max</i>	<i>Min</i>	<i>Mean</i>	<i>Max</i>	<i>Min</i>	<i>Mean</i>	<i>Max</i>
0. Endorheic or Glaciated	86.7	90.5	94.2	512.2	943.9	1367.7	6.1	9.3	15.4
1. Type I Small deltas	93.0	94.9	95.7	196.8	415.6	829.7	10.2	21.4	32.1
2. Type II Tidal systems	94.9	96.2	97.5	222.2	454.9	900.0	9.5	20.2	30.3
3. Type III Lagoons	92.8	95.7	97.3	183.3	530.5	1306.2	6.8	19.9	34.1
4. Type IV Fjords and fjaerds	88.9	90.4	92.2	272.3	414.4	628.4	12.2	18.5	24.8
5. Non-filter Type Va Large Rivers	95.3	97.2	99.2	374.8	2835.6	10204.9	0.9	8.8	20.9
6. Non-filter Type VI Karst	97.0	97.3	97.9	129.5	331.3	857.1	10.1	29.2	42.6
7. Non-filter Type VII Arheic	96.4	97.0	97.3	164.5	481.2	1133.1	7.8	21.9	36.7
51. Non-filter Type Vb Large Rivers with tidal deltas	97.0	98.0	99.4	385.9	1691.5	5361.8	1.8	10.5	20.2

4.3 Flood extent per terrain class

Apart from the coastal typologies, the terrain influences the flood propagation. Based on 15 different classes, presented by Iwahashi et al. (2018), a distinction is made between terrain types. The results are again established for all baseline return periods, for both the Bathtub approach as the LISFLOOD-AC model.

4.3.1 Flooded area per terrain class

For both the Bathtub approach as the LISFLOOD-AC model, the EAFA values per terrain class are presented in Table 4.10.

Table 4.10: EAFA values per terrain class as estimated by the Bathtub approach and the LISFLOOD-AC model, spanning all baseline return periods.

Terrain class	Bathtub EAFA [km ² /yr]	LISFLOOD-AC EAFA [km ² /yr]
1. Steep mountain (rough)	612	25
2. Steep mountain (smooth)	56	3
3. Moderate mountain (rough)	1450	92
4. Moderate mountain (smooth)	68	6
5. Hills (rough in small and large scale)	2542	415
6. Hills (smooth in small scale, rough in large scale)	565	100
7. Upper large slope	20	2
8. Middle large slope	63	12
9. Dissected terrace, moderate plateau	2514	660
10. Slope in and around terrace or plateau	249	70
11. Terrace, smooth plateau	3402	689
12. Alluvial fan, pediment, bajada, pediplain	602	98
13. Alluvial plain, pediplain	2552	471
14. Alluvial or coastal plain, pediplain	11529	2332
15. Alluvial or coastal plain (gentlest), lake plain, playa	8807	704

To visualize the EAFA values, a bar plot is created (Figure 4.17). From this figure it is observed that the largest EAFA values are observed for the same terrain classes by both models, although the magnitude of estimated EAFA differs significantly.

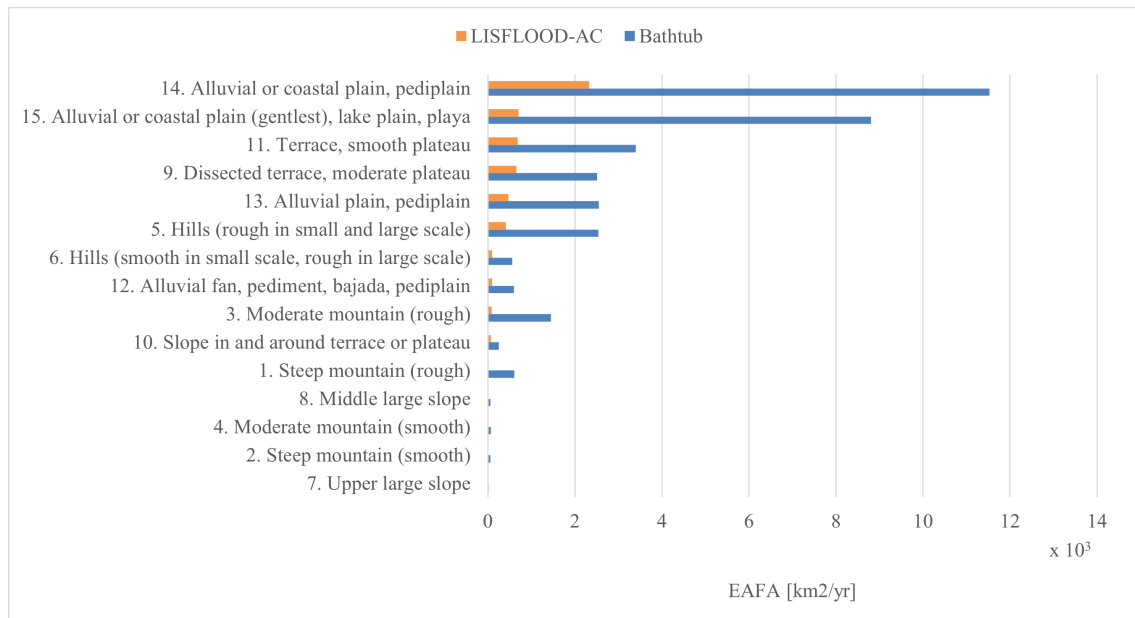


Figure 4.17: Total Estimated Annual Flooded Area (EAFA) per terrain class as estimated by the Bathtub approach and the LISFLOOD-AC model.

The presence of terrain classes is not equally distributed across the globe. Therefore, the EAFA values per terrain class are compared as factor differences. These are computed as the EAFA

as estimated by the Bathtub approach divided by the EAFA as estimated by the LISFLOOD-AC model. A positive value therefore corresponds to overestimation by the Bathtub approach compared to the LISFLOOD-AC model. This results in the bar plot shown in Figure 4.18

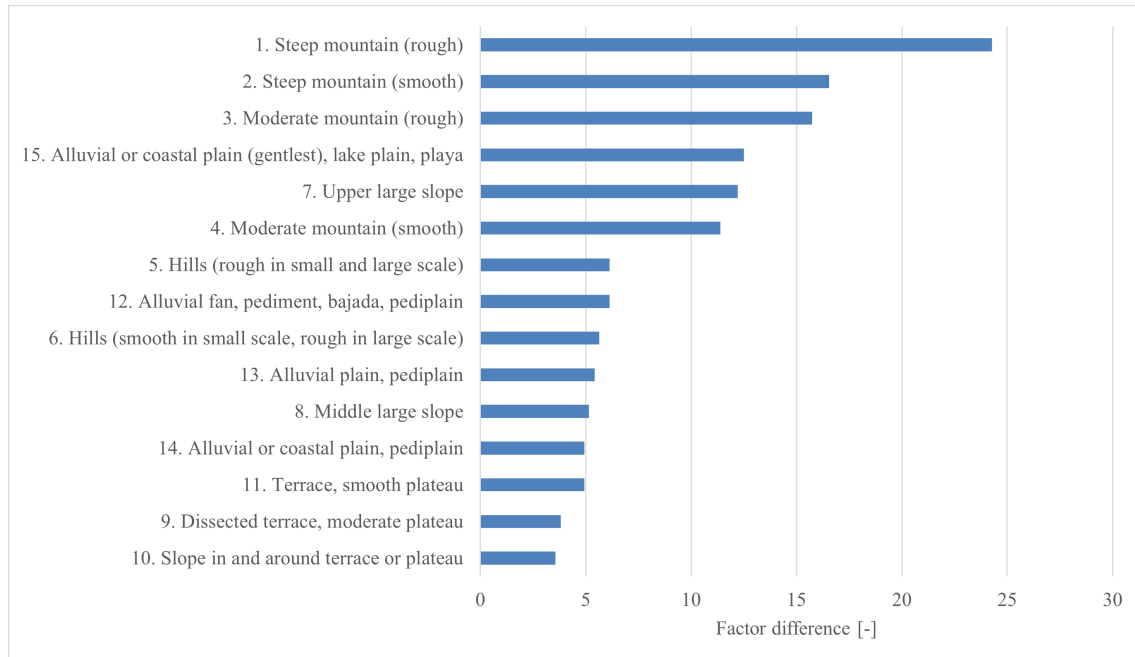


Figure 4.18: Factor difference in total EAFA per terrain class as estimated by the Bathtub approach and the LISFLOOD-AC model for all baseline return periods. This factor difference is computed as (EAFA Bathtub/EAFA LISFLOOD-AC).

The factor difference in EAFA as estimated by the Bathtub approach and the LISFLOOD-AC model is the largest for the terrain class Steep mountain (rough), followed by the class Steep mountain (smooth). The corresponding values of 24.3 and 16.5 respectively, clearly represent a substantial difference in the estimated flooded area. However, the estimated flooded area for these classes is small by both modelling approaches (Table 4.10). The terrain class for which the factor difference in EAFA is the smallest is Slope in and around terrace or plateau, followed by Dissected terrace, moderate plateau; with corresponding values of 3.6 and 3.8 respectively. This implies that the Bathtub approach overestimates the flooded area with at least a factor 3.6 compared to LISFLOOD-AC, based on these terrain classes. Therefore, from these results it can be stated that the Bathtub approach never provides a sufficient estimate of the flooded area for any type of terrain.

The absolute difference and the percentage of this difference to the total global difference in EAFA as estimated by the Bathtub approach and the LISFLOOD-AC model is determined. All these are presented in Table 4.11.

While the factor difference between both models is the largest for Steep mountain (rough) and Steep mountain (smooth), this difference only includes 2.2% of the total global difference in EAFA between both models. The largest contribution to the difference in EAFA comes from the terrain classes of the plain overview group, including Alluvial or coastal plain (gentlest), lake plain, playa; Alluvial or coastal plain, pediplain; and Alluvial plain, pediplain, with a combined value of 66.0%. The propagation of the coastal flood is only limited by the topography in the Bathtub approach, while the LISFLOOD-AC model also incorporates the effect of landscape roughness. Therefore, in flat terrains like plains, the flood propagation in the Bathtub approach experiences no deceleration which causes significant extents of the flood. This especially holds in combination with the fact that the Bathtub approach does not include conservation of mass and therefore assumes an unlimited amount of water that can propagate inland.

Table 4.11: Differences in EAFA (Bathtub - LISFLOOD-AC), factor difference in EAFA (Bathtub/LISFLOOD-AC) and percentage of total difference in EAFA values per terrain class.

Terrain class	Diff. (Bath - LIS) [km ² /yr]	Fact. Diff. (Bath/Lis) [-]	Diff. to total [%]
1. Steep mountain (rough)	587	24.3	2.0
2. Steep mountain (smooth)	52	16.5	0.2
3. Moderate mountain (rough)	1358	15.7	4.6
4. Moderate mountain (smooth)	62	11.4	0.2
5. Hills (rough in small and large scale)	2127	6.1	7.2
6. Hills (smooth in small scale, rough in large scale)	465	5.6	1.6
7. Upper large slope	18	12.2	0.1
8. Middle large slope	51	5.2	0.2
9. Dissected terrace, moderate plateau	1854	3.8	6.3
10. Slope in and around terrace or plateau	179	3.6	0.6
11. Terrace, smooth plateau	2713	4.9	9.2
12. Alluvial fan, pediment, bajada, pediplain	504	6.1	1.7
13. Alluvial plain, pediplain	2081	5.4	7.1
14. Alluvial or coastal plain, pediplain	9197	4.9	31.3
15. Alluvial or coastal plain (gentlest), lake plain, playa	8103	12.5	27.6

4.3.2 Fit metrics

In Table 4.12 an overview of the fit metrics values for all terrain classes is summarised. These include the minimum; mean; and maximum value per terrain class spanning all baseline return periods. The hit rates result in the highest values for terrain classes of the plains group, whereas lower values are observed for mountainous areas and slopes. This implies that the Bathtub approach generally estimates flooding in areas where the LISFLOOD-AC model does as well, especially for plains. The false alarm rates show substantially high values for all terrain classes. This represents large overestimation by the Bathtub approach compared to the estimates of the LISFLOOD-AC model, which is especially observed for classes of the overview groups mountains and slopes. Critical success index values display significantly low values for a number of terrain classes, including Steep mountain (rough), Steep mountain (smooth) and Upper large slope, representing insufficient agreement between the two modelling approaches. However, the critical success index shows relatively low values for all classes. Implying that there is never a sufficient agreement in flooded area estimates by both modelling approaches for any type of terrain.

Table 4.12: Fit metrics for terrain classes. For the metrics Hit rate, False alarm rate and Critical success index the minimum, mean and maximum value are presented, based on all baseline return periods.

Terrain class	Hit rate [%]			False alarm rate [%]			Critical success index [%]		
	Min	Mean	Max	Min	Mean	Max	Min	Mean	Max
1. Steep mountain (rough)	79.8	81.3	83.9	1435.8	2175.9	3234.2	2.4	3.8	5.5
2. Steep mountain (smooth)	83.9	85.8	89.1	950.8	1570.2	2531.1	3.2	5.6	8.5
3. Moderate mountain (rough)	82.0	83.7	86.0	764.1	1245.8	2036.2	3.9	6.8	10.0
4. Moderate mountain (smooth)	86.2	88.4	91.3	348.3	827.7	1711.6	4.8	11.9	20.4
5. Hills (rough in small and large scale)	85.1	86.7	88.6	307.2	535.3	937.8	8.2	15.1	21.8
6. Hills (smooth in small scale, rough in large scale)	89.0	90.7	92.3	254.5	526.7	1027.5	7.9	16.9	26.1
7. Upper large slope	86.8	87.3	88.2	1069.1	1790.1	3175.7	2.7	5.2	7.5
8. Middle large slope	81.6	84.1	86.9	463.1	676.8	1129.9	6.6	11.6	15.4
9. Dissected terrace, moderate plateau	91.1	92.4	93.8	154.0	319.3	623.9	12.7	25.0	37.0
10. Slope in and around terrace or plateau	88.9	90.0	90.8	209.7	372.8	688.6	11.4	21.0	29.3
11. Terrace, smooth plateau	92.8	94.6	95.7	155.1	316.0	632.0	12.8	25.9	37.4
12. Alluvial fan, pediment, bajada, pediplain	94.0	94.7	95.5	190.1	396.4	852.5	9.9	22.5	32.8
13. Alluvial plain, pediplain	94.4	95.6	96.4	157.5	327.4	699.3	11.9	26.1	37.5
14. Alluvial or coastal plain, pediplain	95.6	96.9	97.8	158.1	370.0	788.7	10.8	24.6	37.9
15. Alluvial or coastal plain (gentlest), lake plain, playa	97.5	98.5	99.1	384.2	1044.5	2301.9	4.1	11.6	20.5

5 | Discussion

The meaning and significance of the results of the global comparative assessment between the Bathtub approach and the LISFLOOD-AC model are presented in this chapter. Per phase of the research project the main findings and the meaning of those findings are outlined. This is followed by a comparison with previously performed research on this topic. Subsequently, the limitations of the findings are discussed; including uncertainties in the modelling phase prior to this comparative assessment as well as uncertainties in the methodology and post-processing during the comparison of the model output. The chapter ends with suggestions for further research.

5.1 Findings and reasoning

5.1.1 Country level

The comparison of the flood extent as estimated by both models based on administrative boundaries showed that the Bathtub approach generally overestimates the flooded area compared to LISFLOOD-AC (Section 4.1.3). The degree of overestimation is represented by a total global factor difference (EAFA Bathtub/EAFA LISFLOOD-AC) of 5.9 between both models, ranging from 10.2 for ESLs with a return period of 5 years till 3.0 for 1-in-200 year ESLs. This implies that the Bathtub approach estimates a global EAFA that is 5.9 times larger than the estimate by the LISFLOOD-AC model. In absolute FA (km²), this overestimation is mostly seen for countries in Asia and Oceania. The global spatial pattern in estimated flood hazard is comparable between both models i.e. the largest FA values are estimated for Australia and Asian countries, with the exception of Canada in the LISFLOOD-AC results. The similar global pattern but different magnitude in estimated flooded area implies that the topography, which is the only variable included in the Bathtub approach, determines whether an area will be flooded or not. However, other variables like surface roughness are crucial to estimate the magnitude of the flood extent. When normalizing the FA estimates by the shoreline length of the corresponding country, largest estimates are not represented by Australia and Asian countries anymore but more spread out around the world. The hit rates reveal that there is a sufficient hit by the Bathtub approach in areas where the LISFLOOD-AC model estimates flooding i.e. the Bathtub approach estimates flooding in areas where the LISFLOOD-AC estimates flooding as well (Section 4.1.5). However, the false alarm rate reveals that the Bathtub approach overestimates flooding compared to the LISFLOOD-AC model since large areas are estimated by the Bathtub approach where the LISFLOOD-AC model does not. Low values for the critical success index correspond to an insufficient fit in estimated flooded area by the Bathtub approach, when assuming the LISFLOOD-AC model estimate as the correct one.

5.1.2 Coastal typology

When comparing the estimated flooded area of both models based on the coastal typology, the largest differences are observed for Tidal systems and Small deltas (Section 4.2.1). Comparing factor differences showed the largest differences for Large Rivers with tidal deltas and Large Rivers. However, these two coastal typology classes only sum up to 6.6% of the total global difference in EAFA of both models. The smallest factor differences in EAFA are observed for Karst coasts; and Fjords and fjaerds. Interesting to note is that this still implies a factor difference of 6.1 and 6.5 respectively, implying that the Bathtub approach does not provide adequate results for any type of coastline. Reasoning for the smallest factor differences determined for these classes might be the steepness of the coastline. Both Fjords and fjaerds as Karst coasts are characterised by steep

slopes, which were calculated from the bathymetry in the study by Dürr et al. (2011). Previously performed research revealed this relation with the slope of the coast as well (Vousdoukas et al., 2016). Furthermore, the volume of available flood waters differs between the two models. This is due to the difference in forcing ESL: the static ESL assuming an infinite time span used in the Bathtub approach versus the triangular synthetic hydrograph included in the LISFLOOD-AC model. The potential flood volume is then a variable which is influenced by the timespan of the forcing ESL from the synthetic hydrograph that will result in coastal flooding (i.e. an ESL higher than the elevation of the coast) while for the Bathtub approach there is an unlimited timespan for which the forcing ESL will cause coastal flooding.

The fit metrics revealed a similar outcome as was observed based on country boundaries: high fit rate values, significantly high false alarm rate values and low critical success index values (Section 4.2.2). The observed false alarm rates are the lowest for the Fjords and fjærds and Karst coasts. Since these coastal typologies are characterized by steeper coastline slopes, the topography has a significant impact on the estimated flooding. This results in less overestimation by the Bathtub approach compared to the LISFLOOD-AC model estimates and therefore smaller false alarm rates are established. The critical success index shows relatively low values for all classes. This means that the Bathtub approach estimates are not comparable to those of the LISFLOOD-AC model for any of the typologies considered.

5.1.3 Terrain classes

A division of the flooded area estimates by both models in 15 terrain classes showed that the difference in EAFA is the largest for plains, including alluvial, coastal and pediplains (Section 4.3.1). When comparing the EAFA per terrain class as factor differences (EAFA Bathtub/EAFA LISFLOOD-AC), the difference is the largest for Steep mountains, especially rough mountains. However, this sums up to only 2.2% of the total global difference in EAFA between both models whereas this is 66.0% for plains. The propagation of the coastal flood is only limited by the topography in the Bathtub approach, while the LISFLOOD-AC model also incorporates the effect of landscape roughness. Therefore, in flat terrains like plains, the flood propagation in the Bathtub approach experiences no deceleration which causes significant extents of the flood. This especially holds in combination with the fact that the Bathtub approach does not include conservation of mass and therefore assumes an unlimited amount of water that can propagate inland. The effects of surface roughness would especially be an important factor for areas with a small difference between the forcing ESL and the land elevation, resulting in small flood depths. For these small flood depths, the degree of friction caused by surface roughness is particularly high compared to bigger flood depths (Seenath et al., 2016).

The fit metrics represent similar results as observed for the subdivision on a country level and the coastal typologies: high hit rate values, significantly high false alarm rates and low critical success index values (Section 4.3.2). This implies that the Bathtub approach generally estimates flooding in areas where the LISFLOOD-AC model does as well, especially for plains. The high false alarm rate values represents large overestimation by the Bathtub approach compared to the estimates of the LISFLOOD-AC model, which is especially observed for classes of the overview groups mountains and slopes. The critical success index shows relatively low values for all classes, implying that there is never a sufficient agreement in flooded area estimates by both modelling approaches for any type of terrain.

5.2 Meaning of results

In all of the performed differentiations of the flooded area estimates of both models, the finding is that the Bathtub approach generally provides results with the highest FA values for the same countries, coastal typologies and terrain classes as the LISFLOOD-AC model but with a significantly larger magnitude of estimated flooded area. This implies that the Bathtub approach does not provide any sufficient results when estimating the flooded area. Although the global flood pattern looks relatively similar, this provides just a topographical estimation of potentially flood prone areas. There is no need to perform an analysis using the Bathtub approach to establish this, since information about the forcing ESLs and the land elevation is sufficient to determine these

potentially flood-prone areas. Therefore, the Bathtub approach would only have a topographic function. According to the findings of this study, it appears to be ill-advised to use the Bathtub approach in quantitative assessments of the coastal flood hazard at large spatial scales.

5.3 Relation of findings to previously performed research

Large scale assessments of the Bathtub approach and LISFLOOD-AC model have hardly been performed. Therefore, only a limited comparison is possible between previous studies and the outcomes of this study.

Local scale studies revealed that the static Bathtub approach does overestimate the flood extent compared to (reduced-complexity) dynamic models (Breilh et al., 2013; Gallien, 2016; Seenath et al., 2016). From these studies, an overestimation between a factor of 0.5 and 2 was observed when comparing the static approach to a dynamic one.

Vousdoukas et al. (2016) performed a study on a European scale for four models, including the Bathtub approach and the LISFLOOD-AC model. Results showed that flood extents were overestimated by the Bathtub approach about 1.6 times compared to the LISFLOOD-AC model. This overestimation was especially seen along areas of the coast which are known for their low-lying/mild-slope terrains. Furthermore, the difference in estimated flood extent was observed to vary substantially per country.

One study by Ramirez et al. (2016) compared the Bathtub approach with a dynamical reduced-complexity model which showed that the Bathtub approach overestimated the flood extent, especially in topographically flat regions. Based on two test cases, in France and Myanmar, an overestimation by the Bathtub approach compared with the actual flood of 204% and 99% respectively was observed. Their reduced-complexity dynamic model overall provided more conservative estimates of coastal flooding.

Both Vousdoukas et al. (2016) and Ramirez et al. (2016) concluded that the Bathtub approach overestimates the flood extent compared to a reduced-complexity dynamic model. This overestimation was in both studies the largest for shoreline classes characterized by mildly sloping landscapes. However, the degree of overestimation established in this study is even larger than previously performed research determined. This could be the result of different model set-ups e.g. different forcing water levels or DEMs used with other resolutions and accuracy.

5.4 Limitations of findings

Limitation of the findings both include uncertainty arising from the modelling phase as well as uncertainty arising from post-processing of the model output of both models.

The main uncertainties in the modelling phase are comparable to those from previously performed large scale coastal flooding studies (section 1.1.3). The main uncertainties in this global assessment include the inclusion of flood protection levels, the DEM resolution and accuracy and the probabilistic extreme sea levels. The flood protection levels are included as normative standards i.e. no flooding is allowed when the return period of the forcing ESL is lower than the protection standard. When this protection standard is exceeded, the forcing water level is not blocked by the flood protection anymore and will propagate inland, without any hindrance of flood protection. Related to the flood protection standards is the possible exclusion of structures on the hinterland e.g. river dikes and elevated roads and infrastructure due to the resolution of the DEM. These have an impact on the propagation of the flood, both in lateral direction when moving from the coast as in longitudinal direction when passing e.g. country borders. The DEM used here, the GlobCover 2009 90m resolution DEM by ESA, provides another source of uncertainty. Both its resolution and accuracy have an impact on the estimated flooding by both models. The resolution determines the potential area to be flooded by defining the elevation over a certain area. Furthermore, the accuracy plays a role in this since the mean absolute vertical accuracy of 1.92 m (AIRBUS, 2020) can already have a significant impact in the estimated

flooded area, especially for the the Bathtub approach. Uncertainty also stems from the fact that the LISFLOOD-AC model makes use of a synthetic, triangular hydrograph whereas the Bathtub approach only considers a static ESL. The shape of this hydrograph induces uncertainty to the LISFLOOD-AC approach, with the Bathtub approach neglecting any temporal component of the ESL and therefore assuming an unlimited amount of water being available for flooding up to the ESL elevation.

Uncertainty induced by post-processing of the model output and the methods applied to compare both models include the accuracy of global datasets used. The global datasets used in this study are the GSWE database from the JRC, containing information on the occurrence of surface water and the GADM database containing the administrative boundaries. The accuracy of the GSWE database has an influence on the removal of the surface water from the flooding results. Furthermore, since a threshold value of 80% occurrence of water is used, some recently developed water bodies might be included as flooded area in the results. The accuracy of the GADM boundaries has an impact on the estimated flooded area, since it defines the boundary between land and water. However, for areas with a large tidal range, the exact location of the shoreline is hard to define. This is the case for the North-West coast of Australia, for which high FA values are estimated in this study. This is most likely due to the shoreline position as present in the GADM database.

5.5 Suggestions for further research

By including multiple climate change scenarios, it could be investigated if the change in estimated flooded area between these scenarios is comparable between the Bathtub approach and the LISFLOOD-AC model. This might reveal that the Bathtub approach is still sufficient in estimating differences when moving from baseline to climate change scenarios

In this study, the 'original' Bathtub approach is applied. However, potential improvements of this approach are already available. These include the consideration of a water volume or a so called tilting bathtub. In the former case (i.e. volume integration), hydrographs should be included which come with a potential source of error in the analysis. Reason for this is that a hydrograph has to be designed and no real event is used in the analysis. However, in the 'original' Bathtub approach, no volume of water is included at all and therefore the potential area to be flooded is unlimited. In the latter case, by considering a tilting bathtub, a certain water level reduction is assumed from the source due to attenuation from bed roughness (Vafeidis et al., 2019). Comparing the LISFLOOD-AC model with these advanced types of Bathtub approaches might reveal smaller differences in estimated flood hazard.

6 | Conclusion

The objective of this research project was to investigate global inundation estimations from the Bathtub approach, and to critically compare the approach and results to the outcomes of the more detailed, global scale process-based model LISFLOOD-AC. In this chapter, the answer to the formulated research questions are provided.

1. *How does the Bathtub approach compare to the LISFLOOD-AC model in estimations of the flood extent based on administrative boundaries?*

On a global scale, the Bathtub approach provides a similar coastal flood pattern as the LISFLOOD-AC model i.e. the highest FA values are generally observed for the same countries by both approaches. However, taking the magnitude of flooding into account, the Bathtub approach provides much larger FA estimates compared to the LISFLOOD-AC model for most countries in the world. On a global scale, the Bathtub approach estimates an EAFA that is 5.9 times the EAFA estimated by LISFLOOD-AC. Furthermore, for only six countries the estimated EAFA by Bathtub is smaller than 2.0 times the EAFA estimate by LISFLOOD-AC. The degree of overestimation varies substantially among countries, with a minimum factor difference in EAFA of 1.1 for Syria and a maximum factor difference of 253 for São Tomé and Príncipe.

2. *What are the differences in estimated flood extent based on different coastal typologies and why are these observed?*

Based on the coastal typology classes defined by Dürr et al. (2011), the estimated flooded area by both modelling approaches differed to a substantial extent for all of the typology classes. In absolute values of estimated flooded area (km²) the largest differences are observed for tidal systems and small deltas. The smallest differences are observed for coastline types characterised by steep slopes: Karst coasts; and Fjords and fjaerds. Since these coastal typologies are characterized by steeper coastline slopes, the topography has a significant impact on the estimated flooding. This results in less overestimation by the Bathtub approach compared to the LISFLOOD-AC model estimates. However, the Bathtub approach still overestimates the EAFA for these two classes with a factor 6.1 and 6.5 respectively, compared to LISFLOOD-AC.

3. *What are the differences in estimated flood extent based on different coastal terrain types and why are these observed?*

Using the terrain classes defined by Iwahashi et al. (2018) revealed that the Bathtub approach overestimates the flood extent compared to the LISFLOOD-AC model especially for flatter terrains (alluvial and coastal plains). The total difference in EAFA for these terrain classes sums up to 66% of the total global difference in EAFA between both models. For all terrain classes involved the overestimation by the Bathtub approach is significant, with the lowest factor difference of 3.6 observed for slopes in and around terraces or plateaus. The reason for the significant overestimation in flatter terrains is that flood propagation in the Bathtub approach is only limited by topography while the LISFLOOD-AC model also takes into account surface roughness. Furthermore, the

Bathtub approach assumes an ESL for an unlimited time span and therefore the available flood waters are larger than for the LISFLOOD-AC model in which the flood waters are limited by the temporal component of the forcing water level defined by the synthetic triangular hydrograph.

How does the Bathtub modelling approach compare to the LISFLOOD-AC model in terms of applicability to global scale coastal flood hazard estimation?

In global scale coastal flood hazard mapping, the Bathtub modelling approach overestimates the flooded area significantly compared to the process-based reduced-complexity model LISFLOOD-AC. This holds for most countries on Earth (subquestion 1), every coastal typology (subquestion 2) and every terrain class (subquestion 3). Furthermore, this overestimation was observed for all baseline return periods included, although the factor difference reduced when moving to higher return periods of extreme sea levels. According to the findings of this study, it appears to be ill-advised to use the Bathtub approach in quantitative assessments of the coastal flood hazard at large spatial scales.

Bibliography

- Aerts, J. P., Uhlemann-Elmer, S., Eilander, D. & Ward, P. J. (2020). Comparison of estimates of global flood models for flood hazard and exposed gross domestic product: A China case study. *Natural Hazards and Earth System Sciences*, 20(12), 3245–3260. <https://doi.org/10.5194/nhess-20-3245-2020>
- AIRBUS. (2020). Copernicus DEM Product Handbook (v3.0). (November), 1–38.
- Alfieri, L., Salamon, P., Bianchi, A., Neal, J., Bates, P. & Feyen, L. (2014). Advances in pan-European flood hazard mapping. *Hydrological Processes*, 28(13), 4067–4077. <https://doi.org/10.1002/hyp.9947>
- Bates, P. D. & De Roo, A. P. (2000). A simple raster-based model for flood inundation simulation. *Journal of Hydrology*, 236(1-2), 54–77. [https://doi.org/10.1016/S0022-1694\(00\)00278-X](https://doi.org/10.1016/S0022-1694(00)00278-X)
- Bates, P. D., Horritt, M. S. & Fewtrell, T. J. (2010). A simple inertial formulation of the shallow water equations for efficient two-dimensional flood inundation modelling. *Journal of Hydrology*, 387(1-2), 33–45. <https://doi.org/10.1016/j.jhydrol.2010.03.027>
- Bontemps, S., Defourny, P., Bogaert, E. V., Kalogirou, V. & Perez, J. R. (2011). GLOBCOVER 2009 Products Description and Validation Report. *ESA Bulletin*, 136, 53.
- Breilh, J. F., Chaumillon, E., Bertin, X. & Gravelle, M. (2013). Assessment of static flood modeling techniques: Application to contrasting marshes flooded during Xynthia (western France). *Natural Hazards and Earth System Sciences*, 13(6), 1595–1612. <https://doi.org/10.5194/nhess-13-1595-2013>
- Burke, L., Yumiko, K., Kassem, K., Revenga, C., Spalding, M. & McAllister, D. (2001). *Coastal ecosystems*. World Resources Institute. https://doi.org/10.1007/978-0-387-36699-9{_}_19
- Chen, D., Rojas, M., Samset, B. H., Cobb, K., Diongue Niang, A., Edwards, P., Emori, S., Faria, S. H., Hawkins, E., Hope, P., Huybrechts, P., Meinshausen, M., Mustafa, S. K., Plattner, G. K. & Tréguier, A. (2021). *Framing, Context, and Methods*. In: *Climate Change 2021: The Physical Science Basis. Contribution of Working Group I to the Sixth Assessment Report of the Intergovernmental Panel on Climate Change* (V. Masson-Delmotte, P. Zhai, A. Pirani, S. L. Connors, C. Péan, S. Berger, N. Caud, Y. Chen, L. Goldfarb, M. I. Gomis, M. Huang, K. Leitzell, E. Lonnoy, J. Matthews, T. K. Maycock, T. Waterfield, O. Yelekçi, R. Yu & B. Zhou, Eds.). Press.
- Church, J. A. & Gregory, J. M. (2019). Sea level change. *Encyclopedia of Ocean Sciences*, 493–499. <https://doi.org/10.1016/B978-0-12-409548-9.10820-6>
- Corbella, S. & Stretch, D. D. (2013). Simulating a multivariate sea storm using Archimedean copulas. *Coastal Engineering*, 76, 68–78. <https://doi.org/10.1016/j.coastaleng.2013.01.011>
- Data » Gridded Population of the World (GPW), v4 | SEDAC. (n.d.). <https://sedac.ciesin.columbia.edu/data/collection/gpw-v4/sets/browse>
- Deltares. (2014). Delft3D-FLOW user manual.
- Diaz, D. B. (2016). Estimating global damages from sea level rise with the Coastal Impact and Adaptation Model (CIAM). *Climatic Change*, 137(1-2), 143–156. <https://doi.org/10.1007/s10584-016-1675-4>

- Dottori, F., Martina, M. L. & Figueiredo, R. (2018). A methodology for flood susceptibility and vulnerability analysis in complex flood scenarios. *Journal of Flood Risk Management*, *11*, S632–S645. <https://doi.org/10.1111/jfr3.12234>
- Dürr, H. H., Laruelle, G. G., van Kempen, C. M., Slomp, C. P., Meybeck, M. & Middelkoop, H. (2011). Worldwide Typology of Nearshore Coastal Systems: Defining the Estuarine Filter of River Inputs to the Oceans. *Estuaries and Coasts*, *34*(3), 441–458. <https://doi.org/10.1007/s12237-011-9381-y>
- Egbert, G. D., Bennett, A. F. & Foreman, M. G. (1994). TOPEX/POSEIDON tides estimated using a global inverse model. *Journal of Geophysical Research*, *99*(C12). <https://doi.org/10.1029/94jc01894>
- ESA Data User Element. (n.d.). http://due.esrin.esa.int/page_globcover.php
- Forzieri, G., Feyen, L., Russo, S., Vousdoukas, M., Alfieri, L., Outten, S., Migliavacca, M., Bianchi, A., Rojas, R. & Cid, A. (2016). Multi-hazard assessment in Europe under climate change. *Climatic Change*, *137*(1-2), 105–119. <https://doi.org/10.1007/s10584-016-1661-x>
- Fox-Kemper, B., Hewitt, H. T., Xiao, C., Aðalgeirsdóttir, G., Drijfhout, S. S., Edwards, T. L., Golledge, N. R., Hemer, M., Kopp, R. E., Krinner, G., Mix, A., Notz, D., Nowicki, S., Nurhati, I. S., Ruiz, J., Sallée, J.-B., Slangen, A. B. A. & Yu, Y. (2021). *Ocean, Cryosphere and Sea Level Change. In: Climate Change 2021: The Physical Science Basis. Contribution of Working Group I to the Sixth Assessment Report of the Intergovernmental Panel on Climate Change* (V. Masson-Delmotte, P. Zhai, A. Pirani, S. L. Connors, C. Péan, S. Berger, N. Caud, Y. Chen, L. Goldfarb, M. I. Gomis, M. Huang, K. Leitzell, E. Lonnoy, J. Matthews, T. K. Maycock, T. Waterfield, O. Yelekçi, R. Yu & B. Zhou, Eds.; tech. rep. August). Cambridge University Press.
- GADM. (n.d.). <https://gadm.org/index.html>
- Gallien, T. W. (2016). Validated coastal flood modeling at Imperial Beach, California: Comparing total water level, empirical and numerical overtopping methodologies. *Coastal Engineering*, *111*, 95–104. <https://doi.org/10.1016/j.coastaleng.2016.01.014>
- GDAL — GDAL documentation. (n.d.). <https://gdal.org/>
- Global Airports | Development Data Hub. (n.d.). <https://datacatalog.worldbank.org/search/dataset/0038117>
- Global Ports — WFP GeoNode. (n.d.). https://geonode.wfp.org/layers/esri_gn:geonode:wld_trs_ports_wfp
- Global ports (WFP SDI-T - Logistics Database) - Humanitarian Data Exchange. (n.d.). <https://data.humdata.org/dataset/global-ports>
- Gouldby, B., Méndez, F. J., Guanche, Y., Rueda, A. & Mínguez, R. (2014). A methodology for deriving extreme nearshore sea conditions for structural design and flood risk analysis. *Coastal Engineering*, *88*(June), 15–26. <https://doi.org/10.1016/j.coastaleng.2014.01.012>
- Hallegatte, S., Green, C., Nicholls, R. J. & Corfee-Morlot, J. (2013). Future flood losses in major coastal cities. *Nature Climate Change*, *3*(9), 802–806. <https://doi.org/10.1038/nclimate1979>
- Hanson, S., Nicholls, R., Ranger, N., Hallegatte, S., Corfee-Morlot, J., Herweijer, C. & Chateau, J. (2011). A global ranking of port cities with high exposure to climate extremes. *Climatic Change*, *104*(1), 89–111. <https://doi.org/10.1007/s10584-010-9977-4>
- Hawkes, P. J., Gouldby, B. P., Tawn, J. A. & Owen, M. W. (2002). The joint probability of waves and water levels in coastal engineering. *Journal of Hydraulic Research*, *40*(3), 241–251. <https://doi.org/10.1080/00221680209499940>
- Hinkel, J., Feyen, L., Hemer, M., Cozannet, G., Lincke, D., Marcos, M., Mentaschi, L., Merkens, J. L., Moel, H., Muis, S., Nicholls, R. J., Vafeidis, A. T., Wal, R. S. W., Vousdoukas, M.,

- Wahl, T., Ward, P. J. & Wolff, C. (2021). Uncertainty and bias in global to regional scale assessments of current and future coastal flood risk. *Earth's Future*, 9(e2020EF001882). <https://doi.org/10.1029/2020ef001882>
- Hinkel, J., Lincke, D., Vafeidis, A. T., Perrette, M., Nicholls, R. J., Tol, R. S., Marzeion, B., Fettweis, X., Ionescu, C. & Levermann, A. (2014). Coastal flood damage and adaptation costs under 21st century sea-level rise. *Proceedings of the National Academy of Sciences of the United States of America*, 111(9), 3292–3297. <https://doi.org/10.1073/pnas.1222469111>
- Hinkel, J., Nicholls, R. J., Vafeidis, A. T., Tol, R. S. & Avagianou, T. (2010). Assessing risk of and adaptation to sea-level rise in the European Union: An application of DIVA. *Mitigation and Adaptation Strategies for Global Change*, 15(7), 703–719. <https://doi.org/10.1007/s11027-010-9237-y>
- Hunter, N. M., Bates, P. D., Horritt, M. S. & Wilson, M. D. (2007). Simple spatially-distributed models for predicting flood inundation: A review. *Geomorphology*, 90(3-4), 208–225. <https://doi.org/10.1016/j.geomorph.2006.10.021>
- Hunter, N. M., Horritt, M. S., Bates, P. D., Wilson, M. D. & Werner, M. G. (2005). An adaptive time step solution for raster-based storage cell modelling of floodplain inundation. *Advances in Water Resources*, 28(9), 975–991. <https://doi.org/10.1016/j.advwatres.2005.03.007>
- IPCC. (2012). *Managing the Risks of Extreme Events and Disasters to Advance Climate Change Adaptation. A Special Report of Working Groups I and II of the Intergovernmental Panel on Climate Change* (C. Field, V. Barros, T. Stocker, D. Qin, D. Dokken, K. Ebi, M. Mastrandrea, K. Mach, G.-K. Plattner, S. Allen, M. Tignor & P. Midgley, Eds.). Cambridge University Press. <https://doi.org/10.1017/CBO9781139177245.005>
- IPCC. (2014a). *Climate Change 2014: Impacts, Adaptation and Vulnerability. Part A: Global and Sectoral Aspects. Contribution of Working Group II to the Fifth Assessment Report of the Intergovernmental Panel on Climate Change* (C. Field, V. Barros, D. Dokken, K. Mach, M. Mastrandrea, T. Bilir, M. Chatterjee, K. Ebi, Y. Estrada, R. Genova, B. Girma, E. Kissel, A. Levy, S. MacCracken, P. Mastrandrea & L. White, Eds.). Cambridge University Press. [papers2://publication/uuid/B8BF5043-C873-4AFD-97F9-A630782E590D](https://doi.org/10.1017/CBO9781139177245.002)
- IPCC. (2014b). *Summary for policy makers. In: Climate Change 2014: Impacts, Adaptation, and Vulnerability. Part A: Global and Sectoral Aspects. Contribution of Working Group II to the Fifth Assessment Report of the Intergovernmental Panel on Climate Change*. (C. Field, V. Barros, D. Dokken, K. Mach, M. Mastrandrea, T. Bilir, M. Chatterjee, K. Ebi, Y. Estrada, R. Genova, B. Girma, E. Kissel, A. Levy, S. MacCracken, P. Mastrandrea & L.L. White, Eds.). Cambridge University Press. <https://doi.org/10.1017/cbo9780511976988.002>
- IPCC. (2021). *Summary for Policymakers. In: Climate Change 2021: The Physical Science Basis. Contribution of Working Group I to the Sixth Assessment Report of the Intergovernmental Panel on Climate Change* (V. Masson-Delmotte, P. Zhai, A. Pirani, S. L. Connors, C. Péan, S. Berger, N. Caud, Y. Chen, L. Goldfarb, M. I. Gomis, M. Huang, K. Leitzell, E. Lonnoy, J. Matthews, T. K. Maycock, T. Waterfield, O. Yelekçi, R. Yu & B. Zhou, Eds.). <https://www.ipcc.ch/report/ar6/wg1/>
- Iwahashi, J., Kamiya, I., Matsuoka, M. & Yamazaki, D. (2018). *Global terrain classification using 280 m DEMs: segmentation, clustering, and reclassification* (Vol. 5). Progress in Earth; Planetary Science. <https://doi.org/10.1186/s40645-017-0157-2>
- Jongman, B., Hochrainer-Stigler, S., Feyen, L., Aerts, J. C., Mechler, R., Botzen, W. J., Bouwer, L. M., Pflug, G., Rojas, R. & Ward, P. J. (2014). Increasing stress on disaster-risk finance due to large floods. *Nature Climate Change*, 4(4), 264–268. <https://doi.org/10.1038/nclimate2124>
- Jongman, B., Ward, P. J. & Aerts, J. C. (2012). Global exposure to river and coastal flooding: Long term trends and changes. *Global Environmental Change*, 22(4), 823–835. <https://doi.org/10.1016/j.gloenvcha.2012.07.004>

- Kirezci, E., Young, I. R., Ranasinghe, R., Muis, S., Nicholls, R. J., Lincke, D. & Hinkel, J. (2020). Projections of global-scale extreme sea levels and resulting episodic coastal flooding over the 21st Century. *Scientific Reports*, 10(1). <https://doi.org/10.1038/s41598-020-67736-6>
- Kummu, M., Taka, M. & Guillaume, J. H. (2018). Gridded global datasets for Gross Domestic Product and Human Development Index over 1990-2015. *Scientific Data*, 5(180004), 1–15. <https://doi.org/10.1038/sdata.2018.4>
- Lincke, D. & Hinkel, J. (2018). Economically robust protection against 21st century sea-level rise. *Global Environmental Change*, 51, 67–73. <https://doi.org/10.1016/j.gloenvcha.2018.05.003>
- Matias, A., Ferreira, Ó., Vila-Concejo, A., Garcia, T. & Dias, J. A. (2008). Classification of washover dynamics in barrier islands. *Geomorphology*, 97(3-4), 655–674. <https://doi.org/10.1016/j.geomorph.2007.09.010>
- McCall, R. T., Van Thiel de Vries, J. S., Plant, N. G., Van Dongeren, A. R., Roelvink, J. A., Thompson, D. M. & Reniers, A. J. (2010). Two-dimensional time dependent hurricane overwash and erosion modeling at Santa Rosa Island. *Coastal Engineering*, 57(7), 668–683. <https://doi.org/10.1016/j.coastaleng.2010.02.006>
- McGranahan, G., Balk, D. & Anderson, B. (2007). The rising tide: Assessing the risks of climate change and human settlements in low elevation coastal zones. *Environment and Urbanization*, 19(1), 17–37. <https://doi.org/10.1177/0956247807076960>
- Mentaschi, L., Vousdoukas, M., Voukouvalas, E., Sartini, L., Feyen, L., Besio, G. & Alfieri, L. (2016). The transformed-stationary approach: A generic and simplified methodology for non-stationary extreme value analysis. *Hydrology and Earth System Sciences*, 20(9), 3527–3547. <https://doi.org/10.5194/hess-20-3527-2016>
- Mignot, E., Paquier, A. & Haider, S. (2006). Modeling floods in a dense urban area using 2D shallow water equations. *Journal of Hydrology*, 327(1-2), 186–199. <https://doi.org/10.1016/j.jhydrol.2005.11.026>
- Muis, S., Verlaan, M., Winsemius, H. C., Aerts, J. C. & Ward, P. J. (2016). A global reanalysis of storm surges and extreme sea levels. *Nature Communications*, 7(May). <https://doi.org/10.1038/ncomms11969>
- Neal, J., Schumann, G., Fewtrell, T., Budimir, M., Bates, P. & Mason, D. (2011). Evaluating a new LISFLOOD-FP formulation with data from the summer 2007 floods in Tewkesbury, UK. *Journal of Flood Risk Management*, 4, 88–95. <https://doi.org/10.1111/j.1753-318X.2011.01093.x>
- Neumann, B., Vafeidis, A. T., Zimmermann, J. & Nicholls, R. J. (2015). Future coastal population growth and exposure to sea-level rise and coastal flooding - A global assessment. *PLoS ONE*, 10(3). <https://doi.org/10.1371/journal.pone.0118571>
- New World Bank country classifications by income level: 2020-2021. (n.d.). <https://blogs.worldbank.org/opendata/new-world-bank-country-classifications-income-level-2020-2021>
- Oppenheimer, M. & Glavovic, B. (2019). Chapter 4: Sea Level Rise and Implications for Low Lying Islands, Coasts and Communities. IPCC SR Ocean and Cryosphere. *IPCC Special Report on the Ocean and Cryosphere in a Changing Climate* [H.- O. Pörtner, D.C. Roberts, V. Masson-Delmotte, P. Zhai, M. Tignor, E. Poloczanska, K. Mintenbeck, M. Nicolai, A. Okem, J. Petzold, B. Rama, N. Weyer (eds.)]. In press., Chapter 4 (Final Draft), 1–14.
- Paprotny, D., Morales-Nápoles, O., Vousdoukas, M., Jonkman, S. N. & Nikulin, G. (2019). Accuracy of pan-European coastal flood mapping. *Journal of Flood Risk Management*, 12(2). <https://doi.org/10.1111/jfr3.12459>
- Paprotny, D., Morales-Nápoles, O. & Nikulin, G. (2016). *Extreme sea levels under present and future climate: A pan-European database*. In *3rd European Conference on Flood Risk Management (FLOODrisk 2016)* ([02001], Vol. 7). <https://doi.org/10.1051/e3sconf/20160702001>

- Pekel, J. F., Cottam, A., Gorelick, N. & Belward, A. S. (2016). High-resolution mapping of global surface water and its long-term changes. *Nature*, *540*(7633), 418–422. <https://doi.org/10.1038/nature20584>
- Perini, L., Calabrese, L., Salerno, G., Ciavola, P. & Armaroli, C. (2016). Evaluation of coastal vulnerability to flooding: Comparison of two different methodologies adopted by the Emilia-Romagna region (Italy). *Natural Hazards and Earth System Sciences*, *16*(1), 181–194. <https://doi.org/10.5194/nhess-16-181-2016>
- Poulter, B. & Halpin, P. N. (2008). Raster modelling of coastal flooding from sea-level rise. *International Journal of Geographical Information Science*, *22*(2), 167–182. <https://doi.org/10.1080/13658810701371858>
- Ramirez, J. A., Lichter, M., Coulthard, T. J. & Skinner, C. (2016). Hyper-resolution mapping of regional storm surge and tide flooding: comparison of static and dynamic models. *Natural Hazards*, *82*(1), 571–590. <https://doi.org/10.1007/s11069-016-2198-z>
- Ranasinghe, R., Ruane, A., Vautard, R., Arnell, N., Coppola, E., Cruz, F., Dessai, S., Islam, A., Rahimi, M., Ruiz Carrascal, D., Sillmann, J., Sylla, M., Tebaldi, C., Wang, W. & Zaaboul, R. (2021). *Chapter 12: Climate Change Information for Regional Impact and for Risk Assessment*. In: *Climate Change 2021: The Physical Science Basis. Contribution of Working Group I to the Sixth Assessment Report of the Intergovernmental Panel on Climate Change* (tech. rep.). <https://doi.org/10.1017/9781009157896.014>
- Reisinger, A., Howden, M., Vera, C., Garschagen, M., Hurlbert, M., Kreibiehl, S., Mach, K. J., Mintenbeck, K., O’neill, B., Pathak, M., Pedace, R., Pörtner, H.-O., Poloczanska, E., Rojas Corradi, M., Sillmann, J., Van Aalst, M., Viner, D., Jones, R., Ruane, A. C. & Ranasinghe, R. (2020). *The concept of risk in the IPCC Sixth Assessment Report: A Summary of Cross-Working Group Discussions* (tech. rep. September). Intergovernmental Panel on Climate Change. Geneva, Switzerland.
- Scussolini, P., Aerts, J. C., Jongman, B., Bouwer, L. M., Winsemius, H. C., De Moel, H. & Ward, P. J. (2016). FLOPROS: an evolving global database of flood protection standards. *Natural Hazards and Earth System Sciences*, *16*(5), 1049–1061. <https://doi.org/10.5194/nhess-16-1049-2016>
- Seenath, A., Wilson, M. & Miller, K. (2016). Hydrodynamic versus GIS modelling for coastal flood vulnerability assessment: Which is better for guiding coastal management? *Ocean and Coastal Management*, *120*, 99–109. <https://doi.org/10.1016/j.ocecoaman.2015.11.019>
- Sekovski, I., Armaroli, C., Calabrese, L., Mancini, F., Stecchi, F. & Perini, L. (2015). Coupling scenarios of urban growth and flood hazards along the Emilia-Romagna coast (Italy). *Natural Hazards and Earth System Sciences*, *15*(10), 2331–2346. <https://doi.org/10.5194/nhess-15-2331-2015>
- Serafin, K. A. & Ruggiero, P. (2014). Simulating extreme total water levels using a time-dependent extreme value approach. *Journal of Geophysical Research: Oceans*, *119*, 6305–6329. <https://doi.org/10.1002/2014JC010093>. Received
- Special Flood Hazard Area (SFHA) | FEMA.gov. (n.d.). <https://www.fema.gov/glossary/special-flood-hazard-area-sfha>
- Tamura, M., Kumano, N., Yotsukuri, M. & Yokoki, H. (2019). Global assessment of the effectiveness of adaptation in coastal areas based on RCP/SSP scenarios. *Climatic Change*, *152*(3-4), 363–377. <https://doi.org/10.1007/s10584-018-2356-2>
- The Global Airport Database - By Arash Partow. (n.d.). <https://www.partow.net/miscellaneous/airportdatabase/>
- Tiggeloven, T., De Moel, H., Winsemius, H. C., Eilander, D., Erkens, G., Gebremedhin, E., Diaz Loaiza, A., Kuzma, S., Luo, T., Iceland, C., Bouwman, A., Van Huijstee, J., Ligtvoet, W. & Ward, P. J. (2020). Global-scale benefit-cost analysis of coastal flood adaptation to

- different flood risk drivers using structural measures. *Natural Hazards and Earth System Sciences*, 20(4), 1025–1044. <https://doi.org/10.5194/nhess-20-1025-2020>
- UNDRR. (2019). *United Nations Office for Disaster Risk Reduction*.
- UNFCCC. (1992). United Nations Framework Convention. 62220.
- United Nations Environment Programme (UNEP). (2016). *The Adaptation Finance Gap Report*. <http://web.unep.org/adaptationgapreport/2016>
- Vafeidis, A. T., Nicholls, R. J., McFadden, L., Tol, R. S., Hinkel, J., Spencer, T., Grashoff, P. S., Boot, G. & Klein, R. J. (2008). A new global coastal database for impact and vulnerability analysis to sea-level rise. *Journal of Coastal Research*, 24(4), 917–924. <https://doi.org/10.2112/06-0725.1>
- Vafeidis, A. T., Schuerch, M., Wolff, C., Spencer, T., Merkens, J. L., Hinkel, J., Lincke, D., Brown, S. & Nicholls, R. J. (2019). Water-level attenuation in global-scale assessments of exposure to coastal flooding: A sensitivity analysis. *Natural Hazards and Earth System Sciences*, 19(5), 973–984. <https://doi.org/10.5194/nhess-19-973-2019>
- Vousdoukas, M., Bouziotas, D., Giardino, A., Bouwer, L., Mentaschi, L., Voukouvalas, E. & Feyen, L. (2018a). Understanding epistemic uncertainty in large-scale coastal flood risk assessment for present and future climates. *Natural Hazards and Earth System Sciences*, 18(8), 2127–2142. <https://doi.org/10.5194/nhess-18-2127-2018>
- Vousdoukas, M., Mentaschi, L., Hinkel, J., Ward, P. J., Mongelli, I., Ciscar, J. C. & Feyen, L. (2020). Economic motivation for raising coastal flood defenses in Europe. *Nature Communications*, 11(1). <https://doi.org/10.1038/s41467-020-15665-3>
- Vousdoukas, M., Mentaschi, L., Voukouvalas, E., Bianchi, A., Dottori, F. & Feyen, L. (2018b). Climatic and socioeconomic controls of future coastal flood risk in Europe. *Nature Climate Change*, 8(9), 776–780. <https://doi.org/10.1038/s41558-018-0260-4>
- Vousdoukas, M., Mentaschi, L., Voukouvalas, E., Verlaan, M., Jevrejeva, S., Jackson, L. & Feyen, L. (2018c). Global probabilistic projections of extreme sea levels show intensification of coastal flood hazard. *Nature Communications*, 9(2360). <https://doi.org/10.1038/s41467-018-04692-w>
- Vousdoukas, M., Voukouvalas, E., Mentaschi, L., Dottori, F., Giardino, A., Bouziotas, D., Bianchi, A., Salamon, P. & Feyen, L. (2016). Developments in large-scale coastal flood hazard mapping. *Natural Hazards and Earth System Sciences*, 16(8), 1841–1853. <https://doi.org/10.5194/nhess-16-1841-2016>
- Wahl, T., Haigh, I. D., Nicholls, R. J., Arns, A., Dangendorf, S., Hinkel, J. & Slangen, A. B. (2017). Understanding extreme sea levels for broad-scale coastal impact and adaptation analysis. *Nature Communications*, 8(May), 1–12. <https://doi.org/10.1038/ncomms16075>
- Yamazaki, D., Ikeshima, D., Tawatari, R., Yamaguchi, T., O’Loughlin, F., Neal, J. C., Sampson, C. C., Kanai, S. & Bates, P. D. (2017). A high-accuracy map of global terrain elevations. *Geophysical Research Letters*, 44(11), 5844–5853. <https://doi.org/10.1002/2017GL072874>
- Yunus, A. P., Avtar, R., Kraines, S., Yamamuro, M., Lindberg, F. & Grimmond, C. S. (2016). Uncertainties in tidally adjusted estimates of sea level rise flooding (bathtub model) for the greater London. *Remote Sensing*, 8(5). <https://doi.org/10.3390/rs8050366>

A | Appendices

A.1 Derivation and explanation of coastal typologies

The coastal typologies defined by Dürr et al. (2011) are based on hydrological, lithological and morphological criteria. A brief description and the derivation steps of the different coastal typologies are presented here.

An overview of the coastal typologies is presented in Figure A.1.

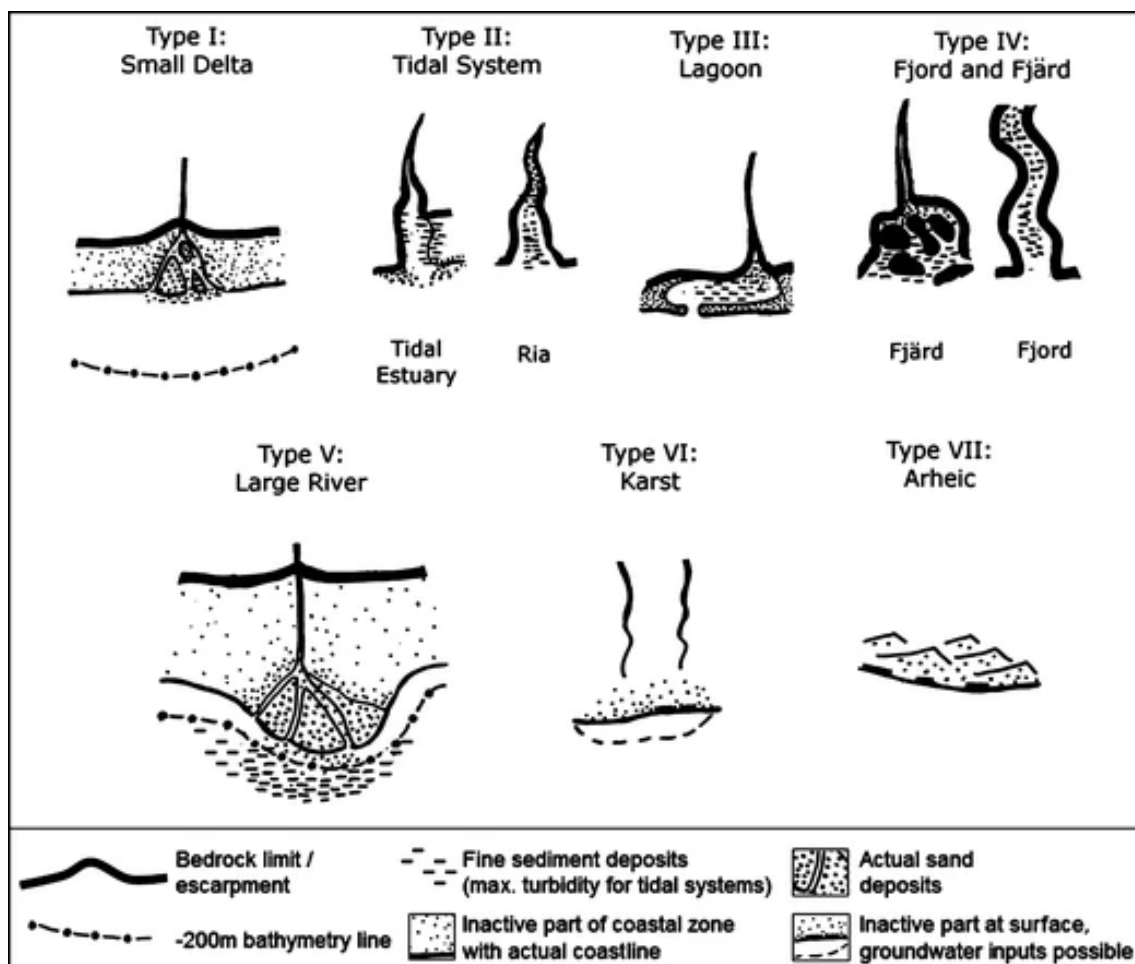


Figure A.1: Estuarine filter types with their physical boundaries, including bedrock limit, the pertaining emerging part of the coast, and fine sediment deposit zones from Dürr et al. (2011).

Small Deltas

Small deltas are defined here as coastal landforms at the mouth of a river, created by sediment deposition. The sediment, supplied to the coastline by a river, is not removed by tides or waves, forming an alluvial landscape.

Tidal Systems

As opposed to the small deltas, tidal systems are river stretches of water that are influenced by the tides.

Lagoons

Coastal lagoons are defined as shallow (generally less than 5 m deep) and elongated water bodies, oriented parallel to the shore. They are characterized by a barrier, separating them from the open ocean.

Fjords and Fjaerds

Fjords and Fjaerds share a glacial origin and are characterised by many islands. Their creation by glaciers resulted in U-shaped valleys with narrow, very steep inlets. Fjaerds are generally wider and shallower compared to Fjords and have more gentle, lateral slopes.

Large Rivers

The sediment delivered by large rivers takes place in a plume on the continental margin, especially at high flow stages, and are therefore classified as non-filter type. These systems can be either tidally influenced or not and therefore a subdivision is established in this coastal typology.

Karst-Dominated Coast

Karst-Dominated Coast cover a system of landforms dominated by dissolution of carbonate rock and consisting primarily of limestone. Due to the effect of both subaerial and marine weathering together with littoral erosion, a typical serrated and peculiar coastline is formed (**Fairbridge1984**).

Arheic Coast

Arheic Coasts are characterised by a near-total absence of river runoff, which is seen in arid regions such as deserts. In this derivation of coastal typologies, arheism is set to an average runoff over the whole watershed of less than 3 mm per year from the continent to the ocean.

The hierarchical steps applied for the determination of the different coastal typologies is presented in Figure A.2.

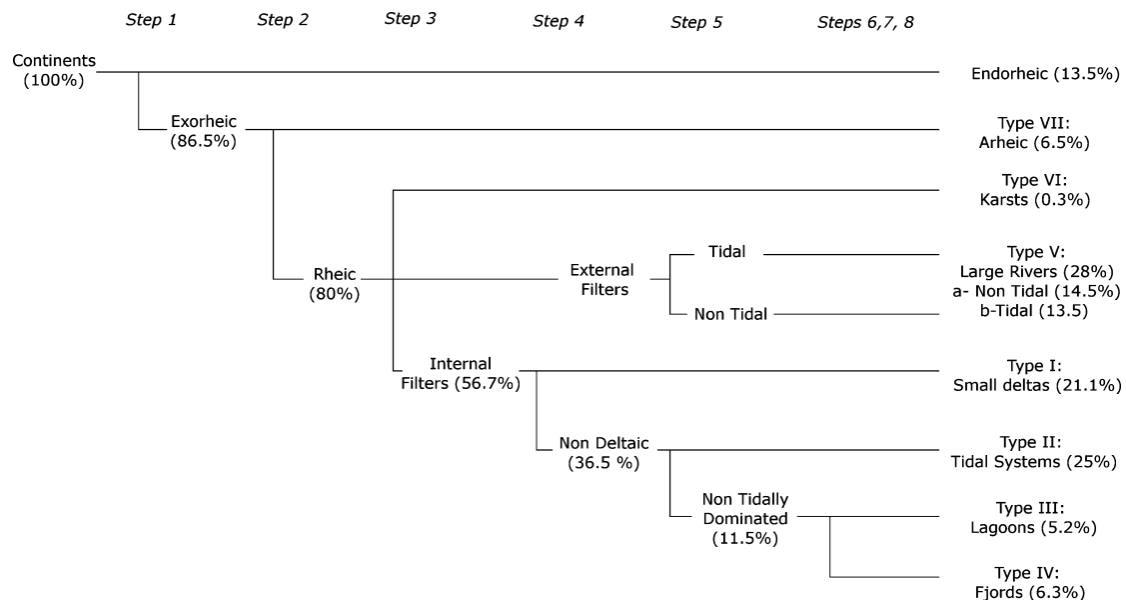


Figure A.2: Decision tree to derive the coastal typologies from Dürr et al. (2011).

Step 1

In the first step, a distinction is made between endorheic and exorheic river basins. In this, endorheic river basins flow towards internal seas and lakes.

Step 2

Step two includes whether a river basin is intercepted by an estuarine filter or not, before entering the ocean.

Step 3

In the third step large rivers are characterized. The smallest large river included is the Rhône River with a discharge of $52 \text{ km}^3/\text{year}$.

Step 4

The remaining smaller deltas, after categorizing the large river areas, are identified in this step. The total delta area for this type is mostly less than 1000 km^2 .

Step 5

Systems that are tidally influenced are derived in this step. This was performed by combining coastline maps showing coastal embayments with global tide amplitude maps.

Step 6

In this sixth step, lagoons were identified. This was performed by a combination of information on the coastline shape and the coastal morphology.

Step 7

Fjords and fjærds are characterized in this step by combining hard rock lithology information with maximum Quaternary glacier coverage extent, and coastline shape and bathymetry.

Step 8

The last step includes the typology derivation for overlapping types. In this, a prioritization is performed as follows (from highest to lowest): large rivers, lagoon, arctic, karst, fjord, tidal systems (estuary and ria), identifiable deltas, fjærd, miscellaneous, mostly remaining stretches of coast (mainly assigned as small deltas).

A.2 Derivation and explanation of terrain classes

The terrain classes as established by Iwahashi et al. (2018) are based on slope gradient, local convexity and surface texture. Applying a machine learning method, *k*-means clustering, resulted in 40 clusters. These clusters were grouped by comparing them with Japanese geological and geomorphological data, reclassifying them into 12 groups with different geomorphological and geological characteristics. Large shape landforms, mountains and hills were subdivided and finally 15 groups were created.

A flowchart of the derivation of the terrain classes is presented in Figure A.3.

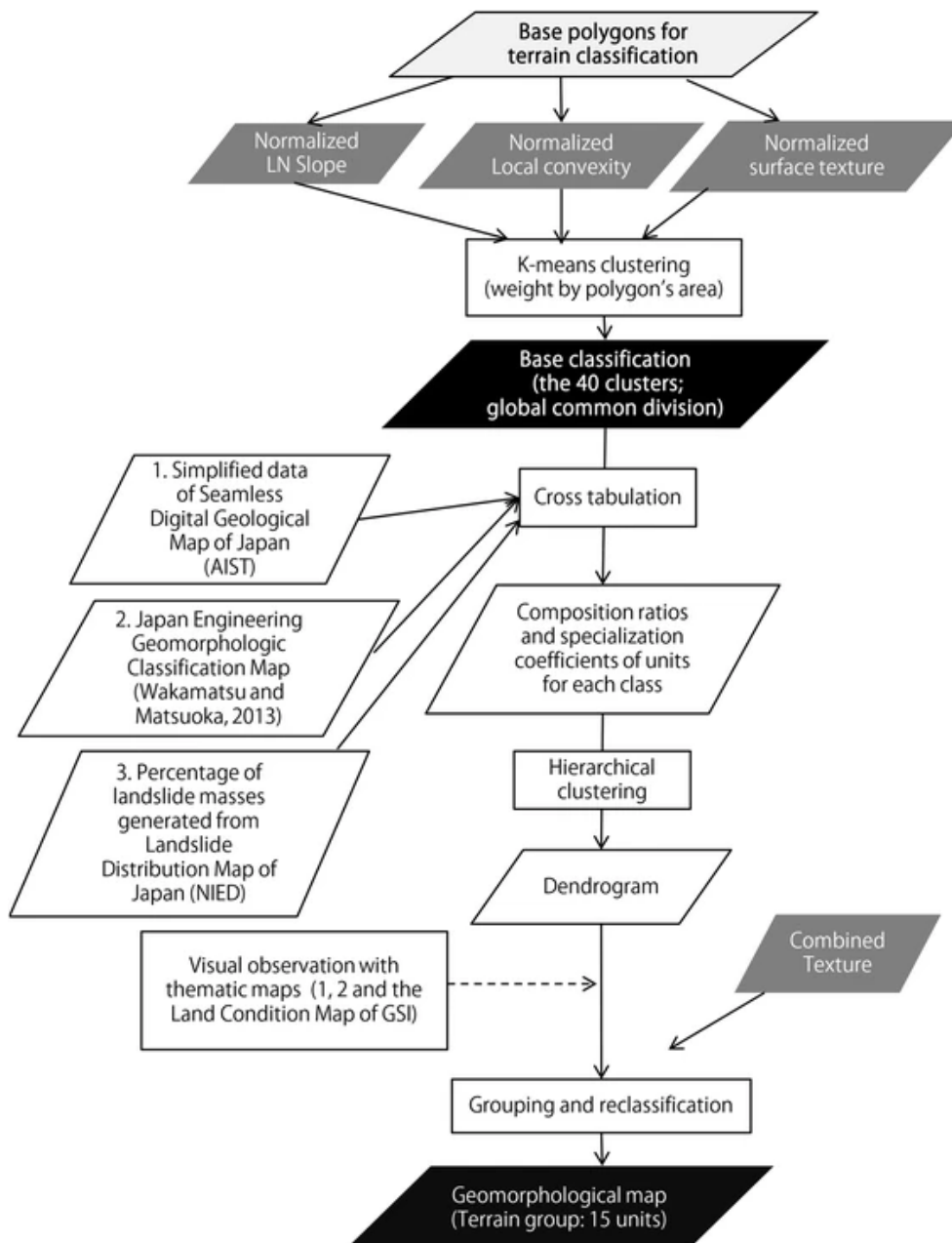


Figure A.3: Flowchart of terrain classification used to generate a geomorphological map from (Iwahashi et al., 2018).

